Journal of the Optical Society of America B
OPTICAL PHYSICS

Quantum nanophotonics in diamond [Invited]

Tim Schröder,[1,*] Sara L. Mouradian,[1] Jiabao Zheng,[1,2] Matthew E. Trusheim,[1] Michael Walsh,[1] Edward H. Chen,[1] Luozhou Li,[1] Igal Bayn,[1] and Dirk Englund[1]

[1]Department of Electrical Engineering and Computer Science, Massachusetts Institute of Technology, Cambridge, Massachusetts 02139, USA
[2]Department of Electrical Engineering, Columbia University, New York 10027, USA
*Corresponding author: schroder@mit.edu

Received 19 January 2016; revised 24 February 2016; accepted 24 February 2016; posted 25 February 2016 (Doc. ID 257648); published 30 March 2016

The past two decades have seen great advances in developing color centers in diamond for sensing, quantum information processing, and tests of quantum foundations. Increasingly, the success of these applications as well as fundamental investigations of light–matter interaction depend on improved control of optical interactions with color centers—from better fluorescence collection to efficient and precise coupling with confined single optical modes. Wide ranging research efforts have been undertaken to address these demands through advanced nanofabrication of diamond. This review will cover recent advances in diamond nano- and microphotonic structures for efficient light collection, color center to nanocavity coupling, hybrid integration of diamond devices with other material systems, and the wide range of fabrication methods that have enabled these complex photonic diamond systems.

OCIS codes: (130.0130) Integrated optics; (160.0160) Materials; (230.0230) Optical devices; (270.0270) Quantum optics.

http://dx.doi.org/10.1364/JOSAB.33.000B65

1. INTRODUCTION

Over the past two decades, color centers in diamond have emerged as promising systems for quantum information (QI) applications [1–3] and precision sensing [4–7]. They were the first and are still among the brightest solid-state, room-temperature single-photon sources [8,9]. Moreover, several defects allow for optical access to associated electron and nuclear spin states, which can exhibit long coherence times [10], enabling their use as quantum memories [11] in QI applications 12]]. These defects also exhibit strong sensitivity to magnetic field [5,13], electric field [14], strain [15], pressure [16], and temperature dependence [17], enabling sensing of small fields at low frequencies [18,19], often at room temperature [20], and down to the single nuclear spin level [21,22]. By coupling these already promising defect centers to optical nano- and microstructures [23–27], one can shape and control the optical properties to increase the performance, efficiency, and fidelity of sensing and QI protocols.

Recent demonstrations of a variety of diamond patterning techniques—focused ion beam (FIB) milling [28], reactive ion etching (RIE) [29–31], quasi-isotropic etching [32], and electron-beam-induced etching [33]—have enabled patterning of diamond at the nanoscale and thus the field of diamond nanophotonics. With high-quality diamond fabrication now a reality, many optical systems have been proposed and realized in diamond and hybrid diamond systems. Here, we will discuss photonic structures for increased collection efficiency, standalone defect cavity systems for tailored light–matter interaction, and hybrid photonic architectures for photon collection, routing, interaction, and detection. We will particularly focus on diamond *photonic* structures coupled to single quantum systems and not discuss diamond plasmonics [34–37], nonlinear photonics in diamond resonators [38], Raman lasers [39], optomechanical systems [15,32,40], and hybrid systems with diamond nanocrystals [41]. While there have been significant advances with nanodiamonds in hybrid photonic systems, and nanodiamond fabrication and properties have advanced [42,43], in this paper we will focus on diamond nano- and microstructures patterned into polycrystalline and single-crystal diamond, which have been shown to have superior optical and spin properties compared to most diamond nanocrystals.

The paper is organized as follows. In Section 2 we briefly introduce the *material properties* of diamond (Section 2.A), followed by *defect centers in diamond* in Section 2.B. In Section 3 we give an overview of various methods for the *fabrication of diamond photonic devices*; in particular, we describe in Section 3.A the *synthetic creation of diamond*, in Section 3.B *diamond thin-film fabrication*, and in Sections 3.C–3.F methods for patterning nano- and microstructures into diamond: *focused ion beam milling*, *direct electron beam lithography*, *transferrable silicon mask lithography*, and *angular etching and isotropic etching techniques*. In Section 4 we introduce various techniques for the

synthetic creation of defect centers, specifically, the influence of *annealing temperature on the optical properties* of defect centers during and after formation in Section 4.A, the *activation of incorporated ions in as-grown diamond* in Section 4.B, the *controlled incorporation of ions during growth* in Section 4.C, the *implantation of ions* in Section 4.D, the *targeted creation of defect centers* in Section 4.E, the *deterministic coupling to optical cavities* in Section 4.F, and a discussion on the *dipole orientation of defect centers* in Section 4.G. In Section 5 we turn our focus to standalone nano- and microstructured *diamond devices for enhanced light collection*, in particular, *waveguide structures* in Section 5.A, *solid immersion lenses* in Section 5.B, and *circular grating structures* in Section 5.C. In Section 6 we discuss standalone *optical cavities in diamond* for enhanced light–matter interaction and control of the emission properties of color centers, in particular, *whispering-gallery-mode resonators* in Section 6.A, *thin-film photonic crystal cavities* in Section 6.B, and *photonic crystal cavities in bulk diamond* in Section 6.C. In Section 7 we discuss *all-diamond photonic systems* as the extension of standalone devices, in particular, *photonic systems in diamond thin films* in Section 7.A and *photonic systems in bulk diamond* in Section 7.B. In Section 8 we elucidate *hybrid photonic systems* consisting in part of a diamond and in part of another material platform, in particular, *hybrid cavity systems* in Section 8.A, *fiber-coupled DBR cavity systems* in Section 8.B, *photonic circuit integration* in Section 8.C, and an outlook toward *complex photonic architectures* in Section 8.D. In Section 9 we *conclude* and discuss the *remaining challenges* for nanofabrication and complex photonic systems.

2. DIAMOND FOR QUANTUM PHOTONICS

A. Material Properties

Diamond's exceptional combination of a wide electronic bandgap, high mechanical strength, high thermal conductivity, and large hole mobility has made it an attractive material for high frequency, power, temperature, and voltage applications such as power electronics [44,45]. Furthermore, diamond is chemically inert and biocompatible making it a promising material for biological applications, especially in nanocrystalline form [46]. In the field of quantum optics, diamond is uniquely attractive due to its wide bandgap, ~5.5 eV, which allows it to host more than 500 optically active defects, known as "color centers." These crystalline defects, corresponding to some combination of displacement or substitution of the native carbon atoms within the diamond lattice, create spatially localized, energetically separated ground and excited states within the electronic bandgap of the bulk crystal. The high Debye temperature of diamond ($\Theta_0 \sim 2219$ K [47]) leads to a relatively low phonon population at room temperature, which allows these defect-related electronic states to persist for long times without suffering from phonon-induced relaxation. Finally, diamond crystals are relatively free of nuclear spins, with a natural composition of ^{12}C of ~99% that can be increased to ~99.99% in isotopically enhanced chemical vapor deposition (CVD) growth [48,49]. This low contribution of ^{13}C background spins leads to low magnetic field fluctuations, in principal facilitating long coherence times for the few electronic or nuclear spins present. These properties make diamond an ideal host material for single quantum defects and photonic elements.

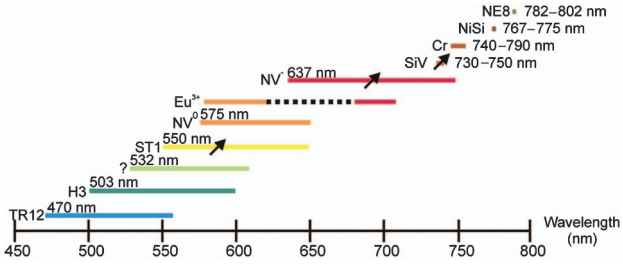

Fig. 1. Overview of studied color centers. For centers with emission wavelengths shorter than 730 nm, the length of the colored line represents the approximate width of the emission spectrum of the color center including phonon sidebands. The wavelength given for each center denotes the ZPL wavelength. The black arrows indicate that the center spin has been addressed. Reprinted with permission from Ref. [51]. Copyright 2014 Optical Society of America.

B. Defect Centers in Diamond

Of the over 500 optically active defect centers in diamond [50], more than 10 have been demonstrated to exist as single quantum emitters [51]. As shown in Fig. 1, these centers span a wide range of single-photon emission wavelengths across the visible spectrum ranging from the blue into the near-infrared.

Of these single-photon sources, three have been observed to exhibit optically detected magnetic resonance (ODMR), in which changes in photon emission intensity are observed while driving the spin on and off resonance with a tunable microwave field, first demonstrated for the negatively charged nitrogen vacancy center (NV–) [52]. This is a convenient mechanism for direct spin state readout via photoluminescence. Spin-state-dependent optical transitions, in general, enable fast initialization, manipulation, and measurement of spin states using laser excitation [12]. Many quantum information processing (QIP) schemes use a link between stationary solid-state quantum memory bits and flying photonic qubits as a basic resource [53], making diamond spin systems an attractive candidate for QIP [1,54].

The most prominent among the ODMR-active diamond color centers is the NV^-, which exhibits stable room-temperature single-photon emission and particularly long electron and nuclear spin coherence times compared to other solid-state defect centers [55]. In the field of quantum optics, the NV^- has notably been applied in experiments demonstrating spin–photon entanglement [56], distant spin entanglement [57], quantum teleportation [58], and finally the first loophole-free demonstration of violating Bell's inequality [59]. Recently, entangled absorption was demonstrated mediated by an inherent spin–orbit entanglement in a single NV^- [60]. Also, the coherent transfer of a photon to a single solid-state nuclear spin qubit with an average fidelity of 98% and storage times over 10 s was demonstrated [61]. In addition to the NV^-, the negatively charged silicon vacancy defect center (SiV^-) has recently gained attention as an optically accessible single-spin system. Notably, the SiV^- in pure, strain-free crystals possesses optical transitions that are naturally nearly lifetime-limited and insensitive to environmental electric noise. This has enabled the

demonstration of high-fidelity Hong–Ou–Mandel interference between photons emitted by two SiV^- centers [62]. Unfortunately, the spin coherence times are currently limited by phonon interactions to several 10 s of nanoseconds, which is many orders of magnitude lower than that of the NV^-.

3. FABRICATION OF DIAMOND PHOTONIC DEVICES

The realization of diamond-based photonic devices requires that optical design parameters are accurately transferred into diamond by either an additive [63] or subtractive approach. We will focus on the subtractive approach, as it is more common for well-designed photonic structures. Various fabrication methods have been used to demonstrate photonic devices in diamond [26,29,30,33,63–66]. FIB milling defines and transfers the photonic pattern directly into diamond [67,68]. Direct electron beam lithography (EBL) writing defines a pattern with nanometer precision in an electron beam resist layer and is usually combined with a subsequent dry etching step to transfer the photonic pattern into the diamond. Transferrable silicon mask lithography [31] exploits the relatively mature fabrication process on silicon-on-insulator (SOI) samples and provides high etch selectivity for the subsequent oxygen etching step of diamond. Due to the lack of commercially available diamond thin films of optical thickness, three-dimensional (3D) monolithic patterning techniques have also been developed such as angular FIB milling, RIE etching [69,70] and isotropic etching [32,71] techniques.

A. Synthetic Creation of Diamond

All successful photonic devices must begin with high-purity single-crystal diamond. While initial defect studies were done on natural diamond, current nanophotonic structures are made from synthetic diamond. CVD and high-pressure high-temperature (HPHT) growth allow for the production of low-strain single-crystal diamond with controllable defect concentrations [45,72]. These high-quality single-crystal diamonds are limited in size to a few tens of mm^2, while polycrystalline films and bulk diamonds can be grown on significantly larger scales, though with less control over lattice strain and defect inclusion across the sample. Growth process parameters strongly influence the quality of the crystal and the concentration and type of lattice defects, making diamond growth still technically challenging, though high-quality synthetic diamonds are available commercially. Ultrapure diamond, categorized as type IIa for low nitrogen and boron content, is often used as a starting point for quantum optics applications because of higher purity. In fact, defects in ultrapure diamond can be eliminated down to levels <1 ppb. However, desired defects can also be introduced in the diamond growth up to high levels >100 ppm, allowing for control of the native defect densities across several orders of magnitude. This approach can avoid crystalline damage associated with defect creation through implantation and has been shown to provide long spin coherence times [73], high defect density, or spatially selected defect layers [74–76] as will be discussed in Section 4.C. Further insights into the synthesis of single-crystal diamond by HPHT or CVD methods, either by homoepitaxial growth [77] or heteroepitaxial deposition on large-area single crystals of a foreign material, are discussed in Refs. [72,78].

B. Diamond Thin-Film Fabrication

Many photonic systems that confine light of the order of the wavelength are based on thin-film substrates which are either suspended or supported by a lower index of refraction material to achieve total internal reflection. For single-mode devices operating resonantly with color centers in the visible range, such a thin film has to be of the order of 200 nm in thickness. In contrast to many other semiconductor materials, single-crystal diamond growth is challenging and has been limited mainly to diamond-on-diamond techniques, precluding the use of an underlying sacrificial layer or lower index material.

One very promising exception is the heteroepitaxial growth via bias-enhanced nucleation [79] on iridium/yttria-stabilized zirconia buffer layers on silicon [layer structure: diamond/Ir/YSZ/Si(001)] [78]. Due to an unmatched degree of initial alignment and extraordinary high density of such epitaxial diamond grains on the iridium layer, they can lose their polycrystalline character during subsequent textured growth within a few to tens of micrometers [80]. A several hundred nanometer thick suspended diamond membrane can be fabricated by first removing the silicon substrate and buffer layers and then dry etching the polycrystalline backside of the diamond [26].

For the fabrication of diamond thin films from bulk diamond substrates, different methods have been developed. FIB milling has been pursued for the separation of small diamond slabs from the bulk [81]. However, the highly physical nature of the ion bombardment causes crystal damage as evidenced by Raman spectroscopy, photoluminescence [81], and transmission electron microscopy [82]. RIE of slabs was seen to cause less crystal damage [82] in the final product, allowing for spin coherence times approaching 100 μs [83]. However, this RIE method only allowed for the production of small ($\sim$10 μm × 10 μm) membranes, which limits the ability to postprocess and fabricate more complex photonic structures.

There has also been work toward the separation of a diamond film from the bulk via ion-slicing (controlled creation of a damage layer). Million electron volt ions accelerated at the diamond crystal will stop at an energy-dependent depth. The damage caused by collisions with the lattice will create a well-localized graphite layer that can be removed via a wet etch step [84,85]. Crystal damage is inevitably induced in the removed membrane. However, this can be mitigated with a strategic etch of the damaged side [86], and subsequent diamond overgrowth [87–89], allowing for high-quality spin properties of defect centers [88].

C. Focused Ion Beam Milling

FIB milling of diamond, in which carbon atoms are mechanically removed from the lattice with accelerated Ga^+ ions or O_2 ions, is a maskless process which can be used for fabrication of diamond photonic devices [26,28,68]. The spatial resolution is mainly limited by the ion beam width. This gives several advantages for diamond patterning: (i) a mask is not required, eliminating the need for special handling or resist spinning, and (ii) optical isolation from the bulk is achieved simply by

tilting the stage to mill at an angle relative to the surface normal and to undercut the structure [28]. FIB milling has been used to demonstrate nanobeam cavities [28] and free-standing, undercut bridge structures [90] in bulk diamond and two-dimensional (2D) photonic cavities [26] in a single-crystal diamond layer on a buffered silicon (Si) substrate. However, this technique is limited by the relatively long milling time and inclined side walls [26], leading to limited cavity quality factors and residual damage to the diamond material, which results in reduced color center properties as well as additional optical and spin background. The material damage from ion milling can be partially removed either by acid treatment and oxidation step [26] or using electron-beam-induced local etching [90]. This minimizes the optical losses and fluorescence background from the ion contamination.

D. Direct Electron Beam Lithography

EBL is widely used for defining patterns with nanometer feature size and is applied in combination with an etching method, most often RIE or inductively coupled plasma (ICP) RIE. EBL typically requires a conductive substrate that is several millimeters in size and an E-beam resist having sufficient etch selectivity with respect to the substrate for the subsequent pattern transfer. These requirements are challenging to satisfy for small, insulating diamond samples. Coating diamond with a conductive layer is widely used to minimize charging during EBL writing. Hydrogen silsesquioxane resist is a high-resolution E-beam resist that can be used to pattern diamond [91]. Its modest intrinsic selectivity to standard diamond RIE etch recipes can be enhanced by postdevelopment electron curing [92]. The etch selectivity can be further enhanced with other mask layers patterned via lift-off or an initial short dry or wet etch step. Such recipes have been used to demonstrate diamond nanowires [30], suspended waveguide and nanobeam cavities [69,70,76], diamond plasmonic apertures [91], and gratings [37].

E. Transferrable Silicon Mask Lithography

To avoid spin-coating small diamond samples and exposing them to electron, ion, or UV radiation, a novel nanofabrication technique [31] was developed as illustrated in Fig. 2. Instead of defining a mask directly on the diamond substrate, a frameless single-crystal silicon membrane mask is prepatterned from (SOI) samples [93–95] and placed onto the diamond substrate silicon using membrane-transfer techniques [31]. This enables pattern transfer with feature sizes down to 10 nm, etch selectivity of over 38 for the subsequent oxygen RIE, and automatic positioning of ion implantation apertures with respect to the photonic structure, as will be discussed in Section 4 with alignment accuracy guaranteed by the EBL writing. For patterning of the silicon masks, high-resolution EBL is applied, in combination with well-developed RIE.

By applying one of two complimentary transfer techniques, one can place both small and large masks on diamond substrates with sizes up to 200 μm × 200 μm and 1 mm × 1 mm, respectively, as required by the sample size to be patterned. For small masks, a pick-and-place method is applied based on micromanipulation with a micropolydimethylsiloxane (PDMS) adhesive attached to a tungsten probe tip. For large masks, a stamping approach is used with a transparent polytetrafluoroethylene sheet [31]. After the pattern is transferred to diamond by oxygen etching, the Si membrane masks are mechanically removed, avoiding solvent-based mask removal procedures on diamond substrates.

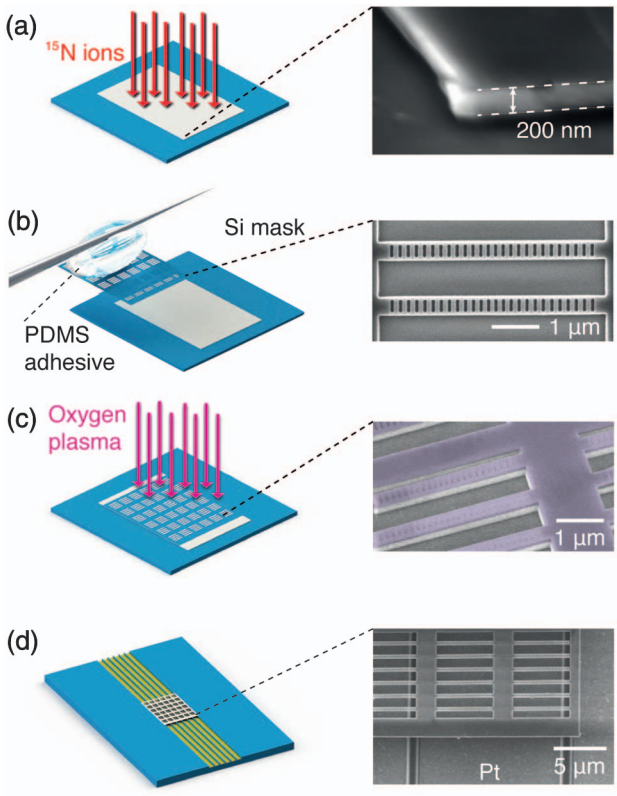

Fig. 2. Fabrication procedure and cavity characterization outcome. (a) NV^-s were created ~100 nm below the surface of the diamond membranes by implantation of ^{15}N atoms and subsequent annealing at 850°C. The magnified scanning electron micrograph (SEM) shows a ~200 nm membrane. (b) Si masks were patterned on silicon-on-insulator and released and transferred onto diamond membranes. The SEM shows a patterned Si mask before transfer. The scale bar represents 1 mm. (c) Oxygen reactive ion etching was used to pattern diamond membranes. The false-color SEM shows the Si mask (purple) on diamond after oxygen etching. The scale bar represents 1 mm. (d) Patterned diamond membrane on microwave striplines for optical and spin characterization. The SEM shows diamond PhC structures alongside metallic striplines in Si channels. The scale bar represents 5 mm. Reprinted by permission from Macmillan Publishers Ltd.: Schröder *et al.*, *Nature Communications*, vol. 6, 6173 (2015) [27]. Copyright 2015.

The Si mask patterning was applied for various photonic nanostructures in both bulk samples [96] and diamond thin films with sizes down to hundreds of square microns [27]. To pattern diamond membranes with 200–300 nm thickness, the diamond membranes are adhered to a Si substrate, the patterned Si mask is put on the diamond membrane using the pick-and-place technique, photonic patterns are transferred into the diamond membrane by oxygen RIE, the Si mask is mechanically removed, and finally isotropic SF_6 plasma is applied to undercut the etched diamond photonic structure for optical measurements.

F. Angular Etching and Isotropic Etching Techniques

As discussed above, the fabrication of large uniform thin-film diamond samples has not yet been developed. This limits the fabrication of diamond devices that guide and capture light when 2D or 3D confinement is required. To achieve the needed optical isolation for photonic structures in bulk diamond, and to circumvent the need for large thin-film diamond samples for patterning, alternative fabrication approaches have been demonstrated that enable the monolithic patterning of waveguide and cavity structures into bulk diamond. One design concept is based on suspended devices with triangular cross sections. Such designs can be realized by angled etching, either by rotating the sample [28] and milling by FIB or by guiding the trajectory of ions with a Faraday cage [69] in an RIE process. Angular etching was used to demonstrate racetrack patterns with an ultrahigh quality factor (Q factor) [69] and one-dimensional (1D) nanobeam cavities [70,96].

Another technique to produce free-standing structures is a quasi-isotropic oxygen undercut. This technique is based on the combination of standard vertical RIE and zero forward bias oxygen plasma etching at an elevated sample temperature. This zero bias etching takes advantage of the low directionality of the oxygen ions and the thermally activated diamond surface leading to a quasi-isotropic chemical etching effect. This technique has enabled high-Q cavities in a nanofabricated photonic disk [32] and high mechanical quality factor waveguides [71].

4. SYNTHETIC CREATION OF DEFECT CENTERS

Color centers can be found in natural or as-grown synthetic diamond. However, for high-quality samples with very low defect concentrations (e.g., N < 1 ppm) the concentration of color centers is too low for many of the intended applications 97]], and the distribution is random. Controlled creation of defect centers is important for the fabrication of photonic constituents in a scalable way and for the extension beyond present proof-of-principle implementations. One can differentiate between methods that rely on (i) "activation" of incorporated defects in as-grown diamond [98], (ii) controlled incorporation of defects during growth [74], and (iii) controlled implantation of defects after diamond growth [99]. Combinations of these methods have also been demonstrated. For example, "activation" methods can be combined with the controlled or targeted "placement" methods [100]. A very powerful tool is the spatially deterministic creation via focused ion beam or masked implantation [101]. These methods enable high yield creation of nanostructures with incorporated defect centers.

The synthetic creation of defect centers depends on a wide range of parameters; annealing temperature, vacancy density, and local charge environment have all been shown to affect NV creation. While many works address NV formation as a function of these parameters, the detailed mechanism of color center creation is still not definitively understood. Until recently, it was commonly proposed that diffusing vacancies are trapped by substitutional atoms (e.g., nitrogen) to create a color center (e.g., the NV) [102–105]. Therefore, the established recipes for creating defect centers rely on annealing above 600°C, at which temperature vacancies become mobile [106,107]. This mechanism has been questioned by advanced density functional theory calculations that were applied to determine the formation and excitation energies, the charge transition levels, and the diffusion activation energies for nitrogen- and vacancy-related defects in diamond [108]. These calculations concluded that irradiation of diamond is more likely to directly create NV defects and not isolated vacancies. Direct NV creation has been shown without thermal annealing by irradiation of diamond that has been implanted with nitrogen ions with low-energy electrons (2–30 keV) [109] and beams of swift heavy ions (~1 GeV, ~4 MeV/u) [110]. However, this model of direct NV creation is contradicted by other works. For example, experimental results still show evidence of high vacancy mobility and indicate formation of NVs after implantation during annealing [111,112]. Further fundamental investigation of defect center creation is required to understand this process in full detail.

A. Annealing Temperature and Optical Properties

Annealing temperatures are a crucial tool to control the concentration of different types of lattice and crystal defects. While it is in principle sufficient to anneal samples just above 600°C, temperatures around 850°C were chosen for most demonstrations over the past years. Recently, temperatures up to 1200°C are being applied to reduce strain and lattice defects, leading to increased spin coherence times of NV^-s [113]. For the SiV^- this leads to a narrowing of the inhomogeneous distribution from 3–4 nm (after 800°C anneal) to 0.03 nm (15 GHz, after 1100°C anneal) and results in nearly lifetime-limited optical linewidths [114]. Furthermore, above 1100°C the concentration of divacancies is reduced as their bonds are broken. Divacancies are suspected to influence the photostability of NV^- centers [108] and spectral diffusion properties of the NV^- ZPL. For N implantation doses of $10^9/cm^2$, energies of 85 keV, and annealing up to 1200°C, stable optical transitions of the NV^- ZPL with linewidths down to 27 MHz have been demonstrated [115], which is close to the lifetime-limited emission linewidth of about ~13 MHz [116]. Charge-state stability has been shown to be directly effected by surface termination, with fluorination leading to a higher concentration of stable NV^- centers [117]. It is commonly assumed that surface treatment also affects the NV^- ZPL stability [115]. However, this has not been systematically studied in the literature at the time of this review.

B. Activation of Incorporated Ions in As-Grown Diamond

Defect centers can be formed by the creation of additional vacancies in doped diamond by irradiation with energetic neutrons, electrons, or ions [98,118,119] in combination with a subsequent annealing step above 600°C. In this process, ions already present in the diamond lattice can be combined with the newly created vacancies.

Early work used electron and Ga^+ beams to irradiate N-rich type-Ib diamond to create vacancies and indirectly defect centers, in particular NV centers, from already incorporated N ions. For an unpatterned diamond surface, a spatial lateral resolution below 180 nm was achieved [98]. Controlling the creation depth relative to the surface is challenging, as lattice

defects are created along the path of the particle in the lattice, and the scattering cross section varies for every species. Scanning focused He-ion irradiation and subsequent annealing was also applied for the creation of NV centers [120,121]. While these works achieve spatially localized NV creation, large areas, in particular entire samples, can also be irradiated to create large ensembles. Such large-area irradiation was, for example, used to create a millimeter-scale diamond sample with about 16 ppm (corresponding to 2.8×10^{18} cm^{-3}) NVs [103]. Such samples with large ensembles of spins enable magnetic field measurements with sensitivities down to <0.5 nT $Hz^{-1/2}$ in the low-frequency regime around 1 Hz [18,20]. For effective sensor volumes of 8.5×10^{-4} mm^3 and ensembles of $N \sim 10^{11}$ NV^-s, photon-shot-noise-limited magnetic field sensitivity was demonstrated with a sensitivity of 0.9 $pT/\sqrt{Hz}$ for ac signals of $f = 20$ kHz.

C. Controlled Incorporation of Ions during Growth: Delta Doping

An alternative way of controlling the depth of defect centers relative to the diamond surface is delta doping. This has been experimentally demonstrated for the NV^- [74] and the SiV^- [75]. For the NV, a nanometer-thick nitrogen-doped layer is created by the controlled introduction of N_2 gas during plasma-enhanced chemical vapor deposition (PECVD) diamond growth. Similarly, SiV^-s are created by controlling the Si concentration during the growth, giving control of the concentration over two orders of magnitude. Subsequent electron irradiation and annealing leads to formation of NV centers in a thin layer. This final NV creation process causes less crystal damage than direct ion implantation methods [113] and is therefore advantageous for both long spin coherence times and stable and narrow spectral linewidths. Delta-doped diamond thin films have been applied to couple ensembles of NV^-s to a nanobeam photonic crystal cavity, demonstrating that this technique could be interesting for single-NV cavity-coupled systems [76]. However, in this work, confinement was demonstrated in 1D only but could be combined with FIB or E-beam "activation" to achieve 3D confinement. For high-resolution sensing in fluids, delta doping enabled engineered diamond probes with diameters and heights ranging from 100 to 700 nm and 500 nm to 2 μm, respectively [122].

Besides incorporating atomic defects into the lattice, the concept of delta doping can also be applied to engineer specific nuclear spin environments, e.g., nanometer-thick layers of ^{13}C in ultrapure natural abundance ^{13}C diamond by switching between purified $^{12}CH_4$ and $^{13}CH_4$ (99.99%) source gases [74] during diamond PECVD growth. This is promising for the creation of a controlled number or distribution of ^{13}C nuclear spin memories, which could be used for spin–spin entanglement, quantum error correction protocols, or quantum simulators [48,123–126].

D. Implantation of Ions

The most common method for the creation of color centers is direct ion implantation of a color center constituent—for example, N, Si, Cr, or other ions [99,127–129]—into the diamond crystal. Subsequent annealing creates defect centers. This method enables control of the center depth with respect to the surface, as can be determined via simulations (the stopping and range of ions in matter, SRIM) [130,131]. The first demonstration of this method used N ions with ∼2 MeV energy, corresponding to an implantation depth of about 1.15 μm [127]. Shallow NV^-s were created with 7 keV ion energy, corresponding to an implantation depth of about 10 nm, and the typical ^{15}N 2-fold hyperfine splitting was demonstrated, in contrast to a 3-fold hyperfine splitting for natural ^{14}N defects [128]. Single-photon emission was demonstrated from single SiV^- centers created via ion implantation of ^{29}Si ions [132]. To further understand the creation process of color centers via ion implantation, the creation efficiency of NVs as a function of ion energy was experimentally determined [104] and compared to theoretical models, leading to 25% NV creation yield per implanted nitrogen ion [133]. All these examples have not demonstrated control of the lateral position of created color centers.

E. Targeted Creation of Defect Centers

The relative alignment of color centers to each other is important for the deterministic arrangement in an array, in particular if these centers are used as a grid of sensors or as a network of entangled spins. Depending on the application, lattice constants as low as tens of nanometers are required with precise positioning at each lattice site. One way to achieve this goal is the targeted implantation through 30 nm apertures in the tip of an atomic force microscope (AFM) [134]. This AFM method was combined with stimulated emission depletion microscopy [135] to demonstrate nanometer-scale mapping of randomly distributed NV^-s within a less than 100 nm diameter spot [136].

A different method for the precise relative alignment of color centers is the implantation through large-scale lithographically defined apertures, for example, EBL written apertures in beam resist [137] or EBL patterned Si masks. In the latter experiment, ensembles of individually resolvable NV^-s were created with nanometer-scale apertures in ultrahigh-aspect-ratio implantation masks. These masks were fabricated by narrowing down apertures via atomic layer deposition (ALD) of alumina, enabling a Gaussian full width at half-maximum (FWHM) spatial distribution of about 26.3 nm, thus reaching the lateral implantation straggle limit [101]; see Fig. 3.

Irradiation is not limited to as-grown diamond but can also be used to increase the creation yield of delta-doped samples. For example, ^{12}C implantation of a delta-doped sample postgrowth, creates additional lattice defects, and individual NV^-s can be localized within a volume of $(180\ nm)^3$ in an unpatterned diamond at a predetermined position defined by an implantation aperture [112]. Alternatively, by combining delta doping for vertical confinement and electron irradiation in a transmission electron microscope for lateral confinement, NV^-s were created in a volume of less than $4\ nm \times 1\ \mu m^2$ [100].

A very versatile tool for the creation of color center arrays is focused ion beam implantation. It is maskless and enables the implantation of almost arbitrary patterns. Similar to the electron beam in an scanning electron microscope, a focused ion beam can be applied to control the position and concentration

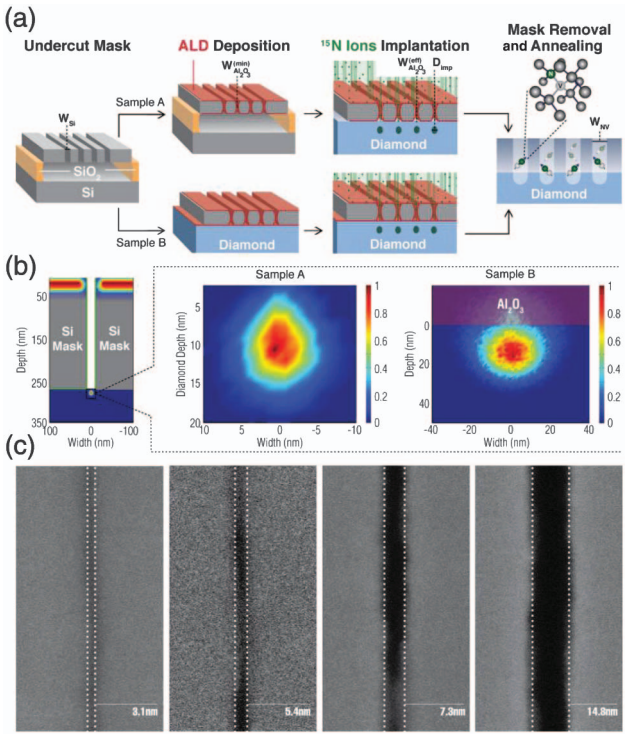

Fig. 3. Implantation through silicon hard mask. (a) Fabrication scheme from silicon mask undercut to implantation for Samples A and B. (b) SRIM simulation of implanted nitrogen. Vertical cross section of the mask and implantation region (left); close-up of nitrogen postimplantation ion on Sample A (center, 6 keV) and Sample B (right, 20 keV) with lateral straggle of 3.1 and 11 nm, respectively. Color bar: normalized nitrogen density. (c) Top-down SEM images of mask following ALD, showing a minimum mask width of 3.1 nm. Reprinted with permission from [Bayn *et al.*, *Nano Letters*, vol. 15, 1751–1758 (2015)] [101]. Copyright 2015 American Chemical Society.

of ions. This method has been used to implant N ions within a spot size of approximately 100 nm [68]. Similarly, arrays of silicon vacancy centers were created by low-energy focused ion beam implantation [138]. These are promising methods toward the targeted coupling of single defect centers to nanostructures.

F. Deterministic Coupling to Optical Cavities

The deterministic coupling of a single or few color centers to a photonic nanostructure, in particular a high-Q cavity, is one of the most important prerequisites for the upscaling of QI architectures. Such deterministic coupling was recently demonstrated by fabrication of a photonic crystal cavity around a precharacterized SiV^- by FIB milling [139], enabling a resonant Purcell enhancement of the zero-phonon transition by a factor of 19, mainly limited by the positioning accuracy. To achieve a higher positioning accuracy, targeted implantation of ions into a photonic crystal cavity was realized with the AFM method discussed earlier, and Purcell enhancement of single NV^- centers was demonstrated [140]. A more scalable fabrication method for cavity-defect center systems is based on an implantation mask with small apertures of 30–70 nm in diameter for targeting a large number of cavity mode maxima with a

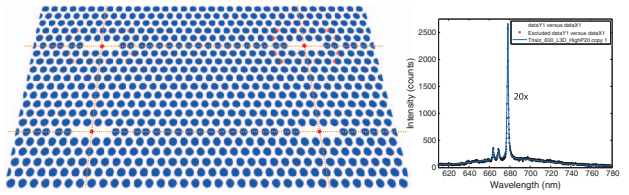

Fig. 4. Targeted creation of single NV^- defect centers in the mode maximum of L3 photonic crystal cavities. The illustration indicates an ideal NV^- cavity system: in the center of each cavity, a single NV^- was created. The spectrum is an example of the experimental implementation that yielded in a high number of NV^- cavity systems. For certain fabrication runs, most of the cavities in large arrays of more then 100 cavities were coupled to a single or few NV^-s and showed intensity enhancement of the phonon sideband by a factor of 5 to 20 [141]. Adapted reprint with permission from Ref. [142]. Copyright 2015 Optical Society of America.

wide ^{15}N beam [141]. By combining the nanocavity etch mask with an implantation mask into a single physical mask, RIE etching (see Section 3) and implantation can be carried out subsequently without the need of challenging realignment processes for two-mask processes. With this method, intensity enhancement of a factor up to 20 was demonstrated (Fig. 4) [142].

G. Dipole Orientation of Defects

To achieve optimal light–matter coupling in cavities and other photonic systems, the defect centers must not only have precise spatial positing with respect to the optical field, but their emission dipoles must also be correctly aligned. Each color center has an individual atom vacancy composition and geometry and therefore a certain emission dipole orientation. For instance, the NV center has four possible orientations with respect to the crystal lattice. Naturally occurring NV populations have a random distribution of orientations. In the last few years, research has been done to control the orientation of NV centers during CVD growth and thus increase the device yield. Initial studies showed that diamond grown with homoepitaxial CVD growth on [110] [143] and [100] [144] oriented substrates mainly supports two NV orientations when the growth parameters are controlled precisely. Further work showed that for NV centers created during CVD of diamond on [111] surfaces, microwave plasma-assisted CVD yields 94% of NV centers along a single-crystallographic direction [145]. A different study showed that 97% perfect alignment can be obtained by controlling the CVD growth parameters precisely [146]. This research is promising, and if the exact mechanisms can be understood and these samples can be made routinely with high yield, this technology can help increase quantum sensing sensitivity as well as interaction with fabricated photonic structures.

5. DIAMOND DEVICES I: ENHANCED LIGHT COLLECTION

In this section, we will focus on micro- and nanophotonic structures to increase the collection efficiency of photons emitted by defect centers. A higher collection efficiency leads to

improved entanglement rates for both emission-based and absorption-based quantum communication applications and also to higher read-out fidelities for quantum sensing applications [147,148]. Without any modification of the diamond surface, the high refractive index (~2.4) of diamond results in a relatively small angle (~24.6°) of total internal reflection at diamond–air interfaces, allowing only a small part of the overall emission to exit the diamond. Even for very shallow NV^-s (several 10 s of nm in depth) relevant for sensing applications, emission into the air is unfavorable due to the directed emission of a dipole into the higher refractive index material [149–151]. To overcome this limitation, a variety of photonic structures have been implemented at the diamond–air interface. A selection of devices and methods is discussed in more detail in this section.

A. Waveguiding Structures

One approach for overcoming limited collection efficiencies at diamond–air interfaces are cylinder- or cone-like structures etched into diamond. Depending on their shape and aspect ratio, they are referred to as diamond microcylinders [29], nanowires [23,30], nanopillars [152], nanobeams [148], or nanowaveguides [153].

Conceptually, these structures are micro- or nanometer-sized single-mode waveguides: the defect couples directly to a single waveguide (WG) mode, while emission into other modes is suppressed. This enables efficient coupling to that specific WG mode. For a relatively narrow emission line of a few nanometers, e.g., the ZPL of an NV^- or SiV^-, the coupling efficiency can be up to 86% [154]. From the WG mode the light is then either launched into free space, bulk diamond, or another guiding photonic structure, enabling high overall collection efficiencies. Such structures can be used as standalone devices as discussed in this section or can be integrated in hybrid photonic circuits and fiber architectures (Section 8).

The first demonstration of microcylinders with the high aspect ratio of 8 (25 for exceptional cases) did not yet consider photonic applications but demonstrated smooth and high-rate reactive ion etching of diamond [29]. Numerical modeling was later used to study the coupling of an NV^- to the optical modes of a nanowire and to determine the optimal nanowire parameters for large photon collection efficiency. For nanowires with diameters of 180–230 nm and for s-polarized dipoles with nanometer emission linewidths, more than 80% of emitted photons can couple to the nanowire mode [30]. Such nanowires were realized in the same work in both bulk single-crystal and polycrystalline diamond and were applied to demonstrate high photon collection efficiencies of an NV^- with a detected photon flux of about 168 ± 37 kcts/s, which is ten times greater than for bulk diamond while using ten times less laser excitation power (~58 μW under the same excitation conditions, objective lens with a numerical aperture of 0.95) [23]. An improvement to about 304 kcts/s photon flux in saturation was achieved with NV^-s located about ~1 μm away from the nanowire end by combining ion implantation and top-down diamond nanofabrication [155].

These experiments were realized on [100]-oriented diamond, where the NV^- dipole is inclined to the nanowire axis, limiting the NV^- dipole coupling to the nanowire mode, hence limiting the overall photon collection efficiency. This limitation was overcome by fabricating such nanostructures on [111]-oriented diamond for which the electric dipole can be in-plane, increasing saturated fluorescence count rates to over 10^6 counts per second [152]. Spin coherence measurements of NV^-s in the sample before and after fabrication demonstrated the quality of their nanofabrication procedure, with average spin coherence times remaining unaffected at ~200 μs. A further study in controlling the shape of nanopillars and its corresponding guiding properties was realized with EBL and inductively coupled plasma RIE with a two-resin technology and the usage of a titanium metal mask [156].

By integrating a nanopillar into a diamond AFM cantilever and additionally positioning a single NV^- at the tip of the nanopillar close to the diamond surface, a robust scanning sensor for nanoscale imaging was realized, demonstrating imaging of magnetic domains with widths of 25 nm and magnetic field sensitivities down to 56 $nT/Hz^{1/2}$ at a frequency of 33 kHz [157]. For high-resolution sensing in fluid, cylindrical diamonds particles with diameters (heights) ranging from 100 to 700 nm (500 nm to 2 μm) were fabricated with shallow-doped NV^- centers [122]. The defects in these nanostructures retained spin coherence times >700 μs, enabling an experimental DC magnetic field sensitivity of 9 μT/Hz in fluid.

Nanobeam waveguides with a triangular cross section of 300 nm width and 20 μm length were fabricated as free-standing structures in bulk diamond with an angled reactive ion etching [69] and were placed on a cover slip for oil immersion spectroscopy. By adding 50 nm deep notches every 2 μm along the beam, guided light is scattered to be collected with high numerical aperture (NA = 1.49) collection optics, leading to saturation photon count rates of about 0.95 Mcts/s [148]. These structures were used to demonstrate efficient spin readouts of NV^- centers based on conversion of the electronic spin state of the NV^- to a charge-state distribution, followed by a single-shot readout of the charge state [148].

An asymmetric waveguide design was demonstrated for even higher collection efficiencies for monolithic bulk structures and close to the surface sensing applications [153]. These pillar-shaped nanowaveguides have a top diameter of 400 nm and a bottom diameter of up to 900 nm. This variation modifies the effective refractive index along the pillar as well as the propagation constant for each mode [158], enabling saturation photon count rates of up to ~1.7 Mcts/s. The temperature dependency of the T1 relaxation time of a single shallow NV^- electronic spin was determined with this structure.

B. Solid Immersion Lenses

In contrast to collecting the defect emission via coupling to a waveguide mode, solid immersion lenses (SILs) enable efficient outcoupling from bulk diamond by providing perpendicular angles of incidence at the diamond–air interface. In the simplest implementation, the emission pattern from a color center in diamond is not altered, but a higher fraction of light is emitted into the free space. Although so-called Weierstrass [159] and elliptical [160] designs promise higher collection efficiencies

compared to the standard hemispheric shape, in diamond only hemispheric designs have been realized. One can differentiate between microscopic [161] (a few to a few tens of μm in size) and macroscopic SILs [151].

Microlens arrays were first realized by fabrication of natural diamond by a combination of photoresist reflow and plasma etching with lens diameters ranging from 10 to 100 μm [161]. Concave and convex microlenses with diameters ranging from 10 to 100 μm were fabricated with hot-embossing and photoresist reflow, followed by ICP etching were applied [162].

Microscopic lenses offer the advantage of microintegration and straight-forward fabrication via FIB [24], enabling fabrication around precharacterized defect centers [163]. However, their extraction efficiencies are more sensitive to surface roughness and nonideal shapes than macroscopic lenses. Still, a roughly 10-fold enhancement of the photon detection rate was achieved with 5 μm SILs [24]. Recently, by further optimizing FIB fabrication and alignment parameters, position accuracies of better than 100 nm (lateral) and 500 nm (axial) were demonstrated, leading to saturation count rates of about 1 Mcts/s for a single NV^- center oriented perpendicular to the [111] cut diamond surface [164]. The deterministic alignment relative to color centers, high collection efficiencies, and relative ease of fabrication have made SILs a valuable tool for QI protocols where efficient photon collection is of crucial importance, for example, quantum interference experiments for the heralded entanglement of distant NV^- qubits [57] and unconditional quantum teleportation between them [58].

SILs were also demonstrated for the SiV^- center, enabling higher photon collection efficiencies for fundamental investigations of the electronic structure of the SiV^- [165] and for the demonstration of multiple spectrally identical SiV^- with spectral overlap of up to 91% and nearly transform-limited excitation linewidths [75].

A macroscopic 1 mm in diameter diamond SIL with surface flatness better than 10 nm (rms) was fabricated with a combination of laser and mechanical processing stages, leading to a saturation count rate of 493 kcts/s from a single NV^- [166]. Macroscopic SILs from other materials with high refractive indices such as gallium phosphite (GaP, $n = 3.3$) can also be applied to bulk or thin-film diamond if the surfaces are smooth and flat enough to prevent airgaps of more than a few tens of nm. For thin-film diamond, this leads to a more efficient collection due to the asymmetric refractive index profile around the color center (one side GaP, on the other side air), providing a broadband antenna mechanism for color centers. For a single NV^-, saturation count rates of 633 kcts/s were demonstrated [167].

C. Circular Grating Structure

To further increase the collection efficiency and overall single-photon count rates from standalone photonic devices, a circular "bullseye" grating structure fabricated in a diamond membrane was placed directly on a glass coverslip [168], as indicated in Fig. 5. The periodic grating structure leads to constructive interference of the membrane-guided emission into the out-of-plane direction. Finite-difference time-domain (FDTD) simulations indicate [Fig. 5(c)] that up to 70% of the ZPL

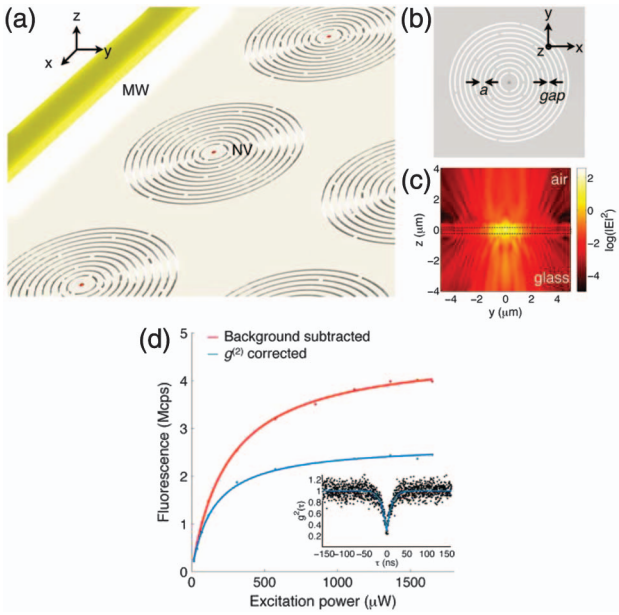

Fig. 5. Bullseye grating structure for high collection efficiency of single defect center emission. (a) Illustration. (b) Parameters of the structure, where a denotes the lattice constant and gap the air spacing between circular gratings. (c) FDTD simulation of the electric field intensity in the $x = 0$ plane with refractive indices corresponding to diamond (bullseye), air (above), and glass (below). Here, $a =$ 330 nm and $gap = 99$ nm. A dipole emitter was placed in the center of the bullseye grating and was oriented along the horizontal direction. (d) Saturation measurements from a single NV^- enhanced by the "bullseye" grating structure in diamond membranes. Reprinted with permission from [Li *et al.*, *Nano Letters*, vol. 15, 1493–1497 (2015)] [168]. Copyright 2015 American Chemical Society.

emission of a horizontally oriented dipole emitter is guided into the glass coverslip, aided in part by the higher refractive index contrast of the diamond–air interface [151]. Fabrication of these devices is carried out with the methods discussed in Section 3. The bullseye gratings were analyzed in a home-built confocal microscope setup (NA = 1.3, Nikon Plan Fluor), and two methods are applied to determine the upper and lower bounds of the saturated single-photon detection rates. As the upper (lower) bound, a single-photon collection rate of about 4.56 Mcps (2.70 Mcps) at saturation was determined. The saturation curves are plotted in Fig. 5(b). Moreover, the high-quality fabrication preserves the spin properties of the included NV^- centers, with measured electron spin coherence times of 1.7 ± 0.1 s [168].

6. DIAMOND DEVICES II: OPTICAL CAVITIES

Optical resonators enable control of the spectral emission properties of optical emitters, and enhancing the light–matter interaction of single-spin systems is enabled by optical resonators. Applying the concepts of optical resonators to diamond photonics allows the tailoring of the light emission properties of defect centers, enhancing their fluorescence emission rates and establishing efficient spin–photon interfaces, particularly important to correlate single spin states with single quantum

states of light. There is also a proposal to improve the efficiency and fidelity of the ground state spin of an NV^- spin using cavity-enhanced reflection measurements [169]. A large variety of resonator types ranging from micro- to nanoscopic designs have been introduced, such as whispering gallery resonators, microscopic open cavity designs, and photonic crystal cavities. A conceptual overview of different cavity designs can be found in a recent review article [170]. The relevant cavity parameters are the cavity quality factor $Q \sim \lambda/\delta\lambda$ and the cavity mode volume V_{mode} which directly influence the dipole–cavity interaction, e.g., the spontaneous emission rate enhancement F_{ZPL} is proportional to $V_{\text{mode}} \sim (\lambda/n)^3$. For a large $F_{\text{ZPL}}^{\max}$ we will focus on photonic crystal (PhC) nanocavities, as they enable small mode volumes [171], $V_{\text{mode}} \sim (\lambda/n)^3$, and large quality factors, Q.

An emitter–cavity system can be described by the Jaynes–Cummings model in the Markov approximation [172], and the Purcell factor quantifies the emitters spontaneous emission (SE) suppression or enhancement [173]. In the strong Purcell regime, in which the emitter is coupled mainly to one optical mode, the SE can be significantly enhanced and the overall Purcell enhancement exceeds one ($F > 1$) [174,175].

When the NV^- ZPL is coupled to a cavity the SE rate is enhanced according to

$$F_{\text{ZPL}} = \xi F_{\text{ZPL}}^{\max} \frac{1}{1 + 4Q^2(\lambda_{\text{ZPL}}/\lambda_{\text{cav}} - 1)^2}, \quad (1)$$

where $F_{\text{ZPL}}^{\max} = \frac{3}{4\pi^2}\left(\frac{\lambda_{\text{cav}}}{n}\right)^3 \frac{Q}{V_{\text{mode}}}$ is the maximum spectrally resolved SE rate enhancement [176] and $\xi = \left(\frac{|\boldsymbol{\mu}\cdot\mathbf{E}|}{|\boldsymbol{\mu}||\mathbf{E}_{\max}|}\right)^2$ quantifies the angular and spatial overlap between the dipole moment ($\boldsymbol{\mu}$) and the cavity mode electric field ($\mathbf{E}$).

In contrast to atoms, quantum dots, and defect centers with narrow emission lines of the order of the cavity linewidth, the NV^- emission has two major contributions: the narrow zero-phonon line (ZPL) emission around 637 nm and a broad phonon sideband emission with a (FWHM) of about 100 nm. The ratio between the two emission bands is described by the Debye–Waller factor DW which is only about 3% for the NV^-. Hence, only a few percent [177] of the overall photoluminescence are emitted into the ZPL. Therefore, one has to differentiate between the overall Purcell enhancement F and the spectrally resolved SE rate enhancement $F_{\text{ZPL}} = F/\text{DW}$ around the ZPL.

A. Whispering Gallery Mode Resonators

In an early demonstration of a whispering gallery mode resonator, diamond microdisks were fabricated into nanocrystalline diamond via FIB milling. Resonant modes with Q-factors of about 100 were observed near the NV^- ZPL around 637 nm via detection of photoluminescence and near 1550 nm via evanescent fiber coupling [178]. Suspended single-crystal diamond microdisks were fabricated by implantation of 180 keV energy boron ions to create subsurface damage, and homoepitaxial diamond overgrowth was applied for required microdisk thickness. The ion-damaged layer was selectively removed by electrochemical etching, and the disks were patterned via ICP-RIE [84]. The first resonant enhancement of the NV^- ZPL was also realized with a single-crystal diamond resonator that was patterned via EBL and oxygen RIE. A 10-fold enhancement was demonstrated, marking an important step of controlling the NV^- emission via coupling to optical resonators [25]. Further work with whispering gallery resonators coupled to waveguides will be discussed in the context of hybrid photonic systems in Section 8.

B. Thin-Film Photonic Crystal Cavities

The first fabrication and optical characterization of photonic crystal cavities were demonstrated with nanocrystalline diamond, and fundamental cavity modes near the NV^- ZPL with Q-factors up to 585 were observed [84]. One-dimensional nanobeam photonic crystal cavities with theoretical Q-factors of up to 10° were introduced and fabricated via two different FIB milling methods [179]. The first demonstration of coupling a single defect center to a PhC cavity was demonstrated by FIB milling of single-crystal diamond for an L7 cavity design and a SiV^- center with fluorescence intensity enhancement by a factor of 2.8 [26]. The demonstration of the 70-fold enhancement of the ZPL transition rate of a cavity-coupled NV^- marked an important step for cavity QED with defect centers in diamond, realized with a photonic crystal cavity fabricated in monocrystalline diamond using standard semiconductor fabrication techniques. The coupled NV^- had a single-scan linewidth of a few GHz, determined with photoluminescence excitation measurements [180]. By coupling a single NV^- to a waveguide-based 1D nanobeam photonic crystal cavity with Q-factors up to 6000, enhancement of the NV^- ZPL fluorescence by a factor of ~7 was demonstrated [181]. Such waveguide-based 1D cavities enable the direct integration into a photonic architecture and are therefore interesting for efficient coupling and transmission experiments. A 1D nanocavity fabricated by transferred hard mask lithography [31] and oxygen RIE (Fig. 6) enabled the demonstration of Q-factors approaching 10,000, enhancement of the ZPL transition rate of ~62, and a beta factor $\beta = 0.54$, indicating operation in the strong Purcell regime [27]. Furthermore, electron spin manipulation was realized for the first time for cavity-coupled NV^-s with coherence times exceeding 200 μs with on-chip microwave striplines for efficient spin control, providing a long-lived quantum system [27]. This spin–photon interface experimentally validates the promise of long spin coherence NV^- cavity systems for scalable quantum repeaters and quantum networks.

C. Photonic Crystal Cavities in Bulk Diamond

Due to the experimental difficulties of creating large-scale, high-quality membranes of uniform and controllable thickness, many groups have begun to explore the fabrication of photonic crystal cavities in bulk diamond. First implementations focused on creating membranes through ion damage of the diamond layer and subsequent etching using FIB milling, as introduced in Section 3.B. This enabled photonic crystals etched from bulk diamond with Q~500 near the NV^- ZPL [182]. However, as discussed previously, the lattice damage in this method is currently high and will most likely hinder the spin and spectral properties of defect centers.

Three-step tilted FIB milling, in which the stage is tilted with respect to the ion milling beam in two directions to

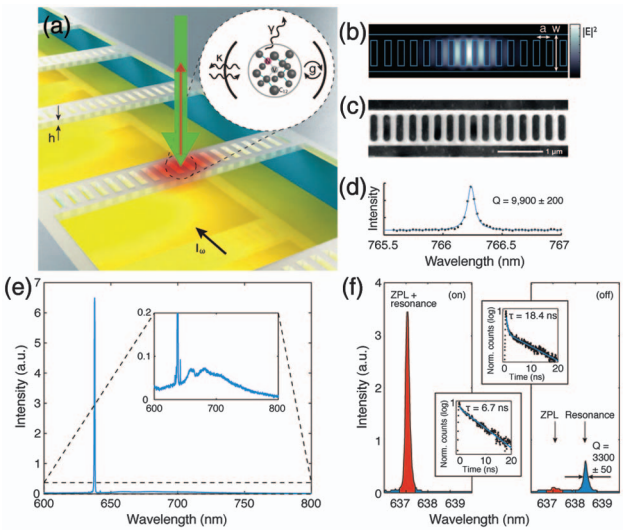

Fig. 6. (a) Diamond PhC cavities are integrated on a Si substrate with metallic striplines for coherent spin control and optically addressed using a confocal set up with 532 nm continuous-wave excitation and photoluminescence collected >630 nm. The inset shows the nitrogen vacancy (NV) nanocavity system with g as the NV^- nanocavity Rabi frequency, γ the NV^- natural SE decay rate, and κ the cavity intensity decay rate. The NV^- consists of a substitutional nitrogen atom adjacent to a vacancy in the diamond lattice. I_0 denotes the current through the stripline and h the membrane thickness. (b) Simulated electric field intensity for the optimized fundamental cavity mode. The PhC has a width W and a lattice constant varying from 0.9a at the center to a ∼220 nm over five periods. (c) Scanning electron micrograph of a representative cavity structure. The scale bar represents 1 mm. (d) Measured cavity resonance (dots) with a quality factor $Q = 9900 \pm 200$ from a Lorentzian fit (blue line). (e) System B at maximum Purcell enhancement. The inset shows a close-up of the spectrum. The ZPL transitions of four individual NV^-s (including the cavity-coupled ZPL) are visible, each with a different strain-induced spectral position. The accumulated phonon sidebands of these NV^-s are also apparent. (f) High-resolution spectra of system B in cavity-coupled and uncoupled cases. The insets show the lifetime measurements corresponding to $\tau_{on} \sim 6.7$ ns and $\tau_{off} \sim 18.4$ ns. Reprinted by permission from Macmillan Publishers Ltd.: Schröder *et al.*, *Nature Communications*, vol. 6, 6173 (2015) [27]. Copyright 2015.

achieve an undercut, and a last untilted mill step is used to etch the photonic crystal holes enabled nanobeam cavities which were separated from the bulk [28,67]. This technology enabled cavities with Qs of a few hundred, matching theoretical predictions across multiple modes [28]. Simulations also showed that the triangular geometry that results from the tilted FIB etching can support high Qs ($>10^6$) [28].

While FIB processing of diamond has enabled cavities in membrane and bulk diamond, it is an inherently low output process, as it is a serial etching process. The development of angled RIE etching with an angled cage allowed the extension of RIE etching techniques to triangular nanobeam cavities in bulk diamond. With this technique, cavities were realized with resonances near the NV^- ZPL of a few thousand [70,96]. High-Q cavities (loaded $Q > 180,000$) have also been demonstrated in the infrared [70].

7. ALL-DIAMOND PHOTONIC SYSTEMS

In contrast to diamond standalone devices, we will discuss diamond photonic systems comprising more than one optical element. This can, for example, be a ring resonator coupled to a waveguide. We make the distinction from standalone devices, as the extension of photonic systems can lead to complex architectures that will enable on-chip functionalities such as generation, entanglement, routing, and gating.

Two approaches have been demonstrated for the fabrication of all-diamond integrated photonic architectures. The first one is based on photonic elements etched into diamond-on-insulator or free-standing diamond thin films. The second approach is based on fabricating monolithic, suspended 3D structures into bulk diamond samples. For more details on the patterning methods, please refer to Section 3.

A. Photonic Systems in Diamond Thin Films

Silicon-on-insulator fabrication technology has enabled many high-quality photonic structures by providing high index contrast and a stable platform. Diamond films suspended over air or placed on SiO_2 substrates provide similar index contrast and stability, and photonic device designs have been shown to translate with ease. The main disadvantage is the requirement of large, single-crystal diamond films with uniform thickness, which are difficult to fabricate as discussed in Section 7.B. Despite this challenge, first proof-of-principle experiments have been demonstrated. Hausmann *et al.* realized a nanophotonic network in a single-crystal diamond film by integrating a high-Q ring resonator ($Q \sim 12,600$) with an optical waveguide containing grating in- and outcouplers. A single NV^- center inside the ring resonator was coupled to its mode, and single-photon generation and routing was demonstrated with an overall photon extraction efficiency of about 10% [183]. In a similar system, Faraon *et al.* showed strong enhancement of the zero-phonon line of NV^- centers coupled to the ring resonance [184]. By replacing grating couplers with polymer spot-size converters at the end of the diamond waveguides, off-chip fiber coupling as low as 1 dB/facet were demonstrated for wavelengths around 1550 nm. The integrated racetrack resonators had quality factors up to ∼250,000, and signatures of nonlinear effects were observed [185]. By coupling a second waveguide to a ring resonator and by locally tuning the temperature of the diamond waveguides, an optical–thermal switch was realized with switching efficiencies of 31% at the drop and 73% at the through port [186].

B. Photonic Systems in Bulk Diamond

Initial attempts to fabricate photonic components in bulk diamond used a combination of patterning techniques (ion-induced damage for structure undercut, RIE for large pattern transfer, and FIB for local pattern transfer) [187]. Two mode ridge waveguides in type-1b single-crystal diamond were produced, though the damage caused by the ion implantation suggests that this technique cannot be adopted for quantum technologies.

On the other hand, triangular RIE etching (as introduced in Section 3.F) is well suited to pattern photonic systems into bulk diamond directly. Free-standing components of a photonic

integrated circuit, including optical waveguides and photonic crystal and microdisk cavities, have been fabricated in a proof-of-principle demonstration [69]. It was later shown in simulation that "s-bend" structures can be used in conjunction with the triangular RIE etching to add low-loss connection points to the bulk and thus extend the length of the waveguides [96]. More work will have to be done in this area to increase the structural stability, operation at visible wavelengths, and fabrication yield of these bulk photonic integrated circuits.

8. HYBRID PHOTONIC SYSTEMS

Hybrid photonic systems combine and exploit the advantages of multiple systems to achieve more functionality than any single isolated system. Random assembly, self assembly, bottom-up fabrication, and manual assembly have all been used to access plasmonic and photonic regimes that would otherwise be inaccessible [41]. Here, we will review the integration of diamond with other semiconductor material systems to gain access to high-quality cavity and photonic integrated circuit systems that are currently difficult to achieve with high yield in diamond. Integration into cavities has allowed for emission enhancement of defects in unpatterned diamond slabs and nanodiamonds [188], and integration into waveguides has allowed for high collection efficiency and on-chip routing of emitted light.

A. Cavity Systems

Due to its large bandgap, low intrinsic fluorescence, and ease of fabrication, gallium phosphide (GaP) has been used to enhance single-defect emission in diamond. The float down of prepatterned GaP microdisks onto an unpatterned bulk diamond allowed GaP to be used as both an etch mask and a higher index guiding material [189]. These high-quality hybrid cavities supported whispering gallery mode resonances with $Q > 25,000$ and loaded Q factor of 3800 [190]. The structure and the mode profile can be seen in Fig. 7. However, the placement of NV^-s with respect to the optical mode is random, and single NV^- enhancement was not shown. The same float down method was used to pattern ring resonators ($Q \sim 3000$–6800) on a diamond sample with a lower density of NV^- centers [191,192]. Tuning the cavity resonance at 10 K and measuring the cavity-coupled emission through a tapered fiber showed enhancement of multiple single NV^- ZPLs. However, the Purcell effect was limited to $F \sim 3.5$, again due to placement with respect to the mode maximum, as well as the large volume of the resonator.

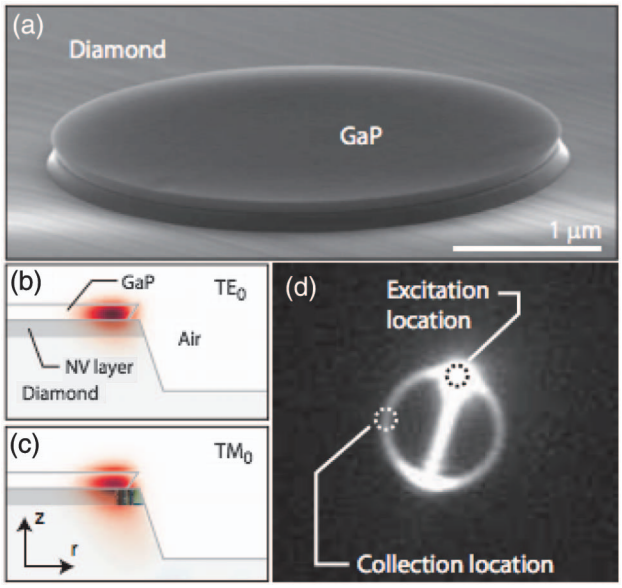

Fig. 7. (a) SEM image of a hybrid GaP–diamond microdisk. (b), (c) FDTD simulated field profiles [$E_r(r,z)$ and $E_z(r,z)$, respectively], of the TE_0^m and TM_0^m modes. (d) Widefield CCD image of photoluminescence from a hybrid microdisk. Reprinted with permission from Ref. [189].

Silica whispering gallery mode (WGM) resonators have also been coupled to diamond structures with NV^- centers in order to exploit the ultrahigh quality factors possible with WGMs, although the mode volumes are high. A deterministic coupling approach in which silica microspheres are brought into contact with integrated 200 nm diamond nanopillars with nanometer precision allows the preservation of NV^- bulk properties while maintaining high quality factors ($Q > 10^6$) for the composite system [193].

B. Fiber-Coupled DBR Cavity Systems

High quality factor resonators can also be achieved with distributed Bragg reflector (DBR) cavities. Microfabricated mirrors can facilitate high finesse, small mode volume cavities which are tunable postfabrication [194–197]. Integrating these DBR mirrors into a fiber-based system maintains the cavity properties, while achieving high coupling into a usable single fiber mode [198]. The coupling of a single NV^- center in a nanodiamond to the field maximum of a tunable high-finesse DBR cavity ($F = 3500$ at 640 nm) via lateral positing allowed the study of the phonon-assisted transitions of the NV^- [199]. A similar setup with a fiber-based DBR cavity elucidated the full scaling laws of Purcell enhancement for the NV^- emission spectrum [200]. Both setups are projected to reach the strong Purcell regime at cold temperatures when the coupling between the NV^- ZPL and the cavity field is larger. A fiber-based DBR cavity in which both input and output are coupled directly to fiber modes has increased the spectral photon rate density by orders of magnitude [201], an important step for quantum information processing. These fiber-based DBR cavities have also been engineered to maintain high finesse and quality factors ($F = 17,000$ $Q \sim 10^6$), even while containing thick diamond membranes (>10 μm) which can contain spectrally stable NV^- centers with long coherence times, unlike nanodiamonds [202].

C. Photonic Circuit Integration

Hybrid systems have also been used to enhance the coupling of the NV^- emission into traveling wave modes for enhanced detection rates and collection into photonic modes that can be then manipulated and interfered to create larger networks. Early work has concentrated on the hybrid diamond–GaP systems discussed in Section 8.A, demonstrating the evanescent coupling of NV^- center emission to GaP multimode

waveguides which suffered from high loss and fluorescence [203]. Theoretical work demonstrated the possibility of single-mode operation with better coupling between the NV^- emission and the GaP waveguide mode, along with a scheme for coupling NV^- centers more than 50 nm from the center to high-Q nanobeam cavities in the GaP layer [204]. Recent work on GaP–diamond hybrid systems has shown the waveguide coupling of single NV^- zero-phonon line emission into disk resonators with estimated high zero-phonon line emission rates into one direction of the waveguide [205]. This approach takes advantage of well-established thin-film growth of and patterning methods of GaP and enables the use of mainly unpatterned diamond to preserve the defect properties. However, this approach is limited by the reduced coupling of the defects to the waveguide mode. While this is mediated by the addition of a cavity as theoretically [204] and experimentally [205] demonstrated, there exists no proposed way to locate the defect in the cavity mode maximum.

One approach to overcome this limitation is to fabricate diamond single-mode waveguides with NV^-s directly at the mode maximum. Such a waveguide can then be coupled with almost unity coupling efficiency to a prefabricated SiN photonic waveguide architecture with a suspended coupling region, as shown in Fig. 8. For a diamond waveguide with a 200 nm × 200 nm cross section, it was determined that a dipole oriented perpendicularly to the propagation direction will couple 83% of the emission to the single optical waveguide mode. Moreover, with the optimized tapering of both the diamond waveguide and the waveguide in the underlying photonic circuitry, up to 96% of the light in the diamond waveguide will be coupled to the single-mode SiN waveguide. In experiment, the hybrid structure shows that 3.5 times more photons emitted by the NV^- are collected into one direction of the waveguide than into a free-space 0.95 NA objective, even with nonoptimized diamond tapering regions [154]. A similar hybrid approach can also be used to efficiently couple light from single emitters in diamond to single-mode silica fibers. As in the photonic integrated circuit, tapers enable an adiabatic mode transfer between the single-mode diamond waveguide and the guided mode in the tapered silica fiber, theoretically enabling unity power transfer from diamond to the fiber waveguide. Experimentally, an overall collection efficiency between 16% and 37% into a single optical mode was demonstrated, with a single-photon count rate of more than 700 kcps in saturation [206].

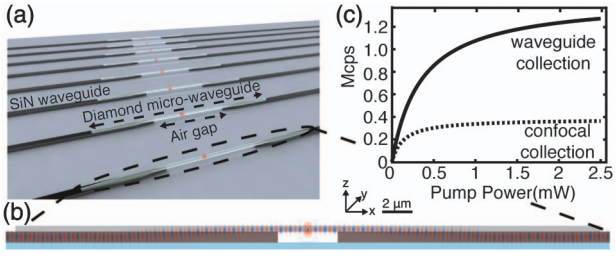

Fig. 8. (a) Sketch of a SiN PIC with multiple quantum nodes. (b) FDTD simulation (E_x field) showing the adiabatic-like mode transfer from a single-mode diamond waveguide into a single mode. (c) Saturation measurements acquired on the same emitter with confocal (dashed line) and waveguide (solid line) collection after background subtraction and correction for measured collection losses. About four times more emission is coupled into the waveguide compared to the high numerical aperture objective. Reprinted with permission from Ref. [154].

D. Toward Complex Photonic Architectures

Another important advantage of a hybrid bottom-up approach is that it enables the building of large-scale systems with almost unity probability, overcoming the stochastic defect center creation process with inherently low yield of high-quality quantum nodes. Preselection of the best diamond waveguides from an array of fabricated waveguides guarantees that every node in the final integrated network will contain a single defect with the desired spectral and spin properties, as well as being well coupled to the optical mode. This enables a linear scaling in the number of fabrication attempts necessary to create a quantum network with the desired number of nodes [154].

To increase the detection efficiency of single photons emitted by defects in diamond, efforts are underway to fabricate superconducting nanowire single-photon detectors (SNSPDs) directly on diamond or to integrate them with hybrid waveguide architectures [207,208]. Niobium titanium nitritide SNSPDs have been fabricated on single-crystal diamond substrates and have been shown to have good detection properties [209]. Niobium nitride (NbN) SNSPDs fabricated directly on waveguides in polycrystalline thin-film diamond grown on oxide show high detection efficiencies up to 66% at 1550 nm combined with low dark count rates and timing resolution of 190 ps [210].

9. CONCLUSION AND REMAINING CHALLENGES

As discussed in this review, recent advances in diamond synthesis and fabrication have enabled high-quality nano- and microphotonic devices for increased photon collection and tailored light–matter interaction. Despite this progress, there are still fundamental challenges to be overcome on the way toward more complex QI implementations based on these diamond photonic nanostructures. High-fidelity QI applications require long spin coherence times and lifetime-limited emission linewidths [53,211,212]. As noted in the review, many diamond growth and fabrication schemes have been tailored to bolster spin coherence times. However, more development must be done to produce nanostructures with both high intrinsic quality (high Q values and low mode volumes) and high defect quality (long spin coherence times and lifetime-limited emission linewidths). In particular, the latter has to date been limited to a factor of about 30 of the fluorescence lifetime limit [154]. It is commonly believed that both crystal lattice defects induced by dry etching and increased surface area near defects due to nanofabrication lead to the degradation of defect properties. Therefore, suitable nanofabrication technology and proper surface termination methods must be developed. Furthermore, the realization of large-scale quantum photonic systems will depend on *scalable fabrication* techniques and on *tunability*—Stark shift control to bring multiple defect transitions (e.g., the NV^- ZPL) to the same frequency [116] and cavity tuning

[213] to match the resonance wavelength with the defect transition frequency without degrading the cavity Q. Finally, for high-fidelity information processing, error correction is required. To establish error-corrected logical qubit nodes in a large quantum photonic processor [214], advances must be made in the high yield creation of coupled defect centers [215] as well as control over the surrounding nuclear environment as a resource to potentially store quantum states longer than an individual quantum memory is able to [125,126,216]. The progress presented in this review proves the viability of diamond-based nanophotonic systems in QI and sensing, and further progress will enable enhanced sensing as well as scalable solid-state quantum networks.

Funding. Air Force Office of Scientific Research (AFOSR) (FA9550-11-1-0014); U.S. Department of Energy (DOE), Office of Basic Energy Sciences (DE-SC0012704); U.S. Army Research Laboratory (ARL) (Center For Distributed Quantum Information).

REFERENCES

1. J. Wrachtrup and F. Jelezko, "Processing quantum information in diamond," J. Phys. **18**, S807–S824 (2006).
2. L. Childress and R. Hanson, "Diamond NV centers for quantum computing and quantum networks," MRS Bull. **38**(02), 134–138 (2013).
3. K. Nemoto, M. Trupke, S. J. Devitt, A. M. Stephens, K. Buczak, T. Nobauer, M. S. Everitt, J. Schmiedmayer, and W. J. Munro, "Photonic architecture for scalable quantum information processing in NV-diamond," arXiv:1309.4277 [quant-ph] (2013).
4. J. Wrachtrup, F. Jelezko, B. Grotz, and L. McGuinness, "Nitrogen-vacancy centers close to surfaces," MRS Bull. **38**(02), 149–154 (2013).
5. S. Hong, M. S. Grinolds, L. M. Pham, D. Le Sage, L. Luan, R. L. Walsworth, and A. Yacoby, "Nanoscale magnetometry with NV centers in diamond," MRS Bull. **38**(02), 155–161 (2013).
6. R. Schirhagl, K. Chang, M. Loretz, and C. L. Degen, "Nitrogen-vacancy centers in diamond: nanoscale sensors for physics and biology," Annu. Rev. Phys. Chem. **65**, 83–105 (2014).
7. L. Rondin, J.-P. Tetienne, T. Hingant, J.-F. Roch, P. Maletinsky, and V. Jacques, "Magnetometry with nitrogen-vacancy defects in diamond," Rep. Prog. Phys. **77**, 056503 (2014).
8. R. Brouri, A. Beveratos, J.-P. Poizat, and P. Grangier, "Photon antibunching in the fluorescence of individual color centers in diamond," Opt. Lett. **25**, 1294–1296 (2000).
9. C. Kurtsiefer, S. Mayer, P. Zarda, and H. Weinfurter, "Stable solid-state source of single photons," Phys. Rev. Lett. **85**, 290–293 (2000).
10. N. Bar-Gill, L. M. Pham, A. Jarmola, D. Budker, and R. L. Walsworth, "Solid-state electronic spin coherence time approaching one second," Nat. Commun. **4**, 1743 (2013).
11. P. C. Maurer, G. Kucsko, C. Latta, L. Jiang, N. Y. Yao, S. D. Bennett, F. Pastawski, D. Hunger, N. Chisholm, M. Markham, D. J. Twitchen, J. I. Cirac, and M. D. Lukin, "Room-temperature quantum bit memory exceeding one second," Science **336**, 1283–1286 (2012).
12. W. B. Gao, A. Imamoglu, H. Bernien, and R. Hanson, "Coherent manipulation, measurement and entanglement of individual solid-state spins using optical fields," Nat. Photonics **9**, 363–373 (2015).
13. J. R. Maze, P. L. Stanwix, J. S. Hodges, S. Hong, J. M. Taylor, P. Cappellaro, L. Jiang, M. V. G. Dutt, E. Togan, A. S. Zibrov, A. Yacoby, R. L. Walsworth, and M. D. Lukin, "Nanoscale magnetic sensing with an individual electronic spin in diamond," Nature **455**, 644–647 (2008).
14. F. Dolde, H. Fedder, M. W. Doherty, T. Nöbauer, F. Rempp, G. Balasubramanian, T. Wolf, F. Reinhard, L. C. L. Hollenberg, F. Jelezko, and J. Wrachtrup, "Electric-field sensing using single diamond spins," Nat. Phys. **7**, 459–463 (2011).
15. P. Ovartchaiyapong, K. W. Lee, B. A. Myers, and A. C. B. Jayich, "Dynamic strain-mediated coupling of a single diamond spin to a mechanical resonator," Nat. Commun. **5**, 4429 (2014).
16. J. Cai, F. Jelezko, and M. B. Plenio, "Hybrid sensors based on colour centres in diamond and piezoactive layers," Nat. Commun. **5**, 4065 (2014).
17. P. Neumann, I. Jakobi, F. Dolde, C. Burk, R. Reuter, G. Waldherr, J. Honert, T. Wolf, A. Brunner, J. H. Shim, D. Suter, H. Sumiya, J. Isoya, and J. Wrachtrup, "High-precision nanoscale temperature sensing using single defects in diamond," Nano Lett. **13**, 2738–2742 (2013).
18. H. Clevenson, M. E. Trusheim, C. Teale, T. Schröder, D. Braje, and D. Englund, "Broadband magnetometry and temperature sensing with a light-trapping diamond waveguide," Nat. Phys. **11**, 393–397 (2015).
19. T. Wolf, P. Neumann, K. Nakamura, H. Sumiya, T. Ohshima, J. Isoya, and J. Wrachtrup, "Subpicotesla diamond magnetometry," Phys. Rev. X **5**, 041001 (2015).
20. D. Le Sage, L. M. Pham, N. Bar-Gill, C. Belthangady, M. D. Lukin, A. Yacoby, and R. L. Walsworth, "Efficient photon detection from color centers in a diamond optical waveguide," Phys. Rev. B **85**, 121202 (2012).
21. J. M. Taylor, P. Cappellaro, L. Childress, L. Jiang, D. Budker, P. R. Hemmer, A. Yacoby, R. Walsworth, and M. D. Lukin, "High-sensitivity diamond magnetometer with nanoscale resolution," Nat. Phys. **4**, 810–816 (2008).
22. I. Lovchinsky, A. O. Sushkov, E. Urbach, N. P. D. Leon, S. Choi, K. D. Greve, R. Evans, R. Gertner, E. Bersin, C. Müller, L. McGuinness, F. Jelezko, R. L. Walsworth, H. Park, and M. D. Lukin, "Nuclear magnetic resonance detection and spectroscopy of single proteins using quantum logic," Science **351**, 836–841 (2016).
23. T. M. Babinec, B. J. M. Hausmann, M. Khan, Y. Zhang, J. R. Maze, P. R. Hemmer, and M. Lončar, "A diamond nanowire single-photon source," Nat. Nanotechnol. **5**, 195–199 (2010).
24. J. P. Hadden, J. P. Harrison, A. C. Stanley-Clarke, L. Marseglia, Y. L. D. Ho, B. R. Patton, J. L. O'Brien, and J. G. Rarity, "Strongly enhanced photon collection from diamond defect centers under microfabricated integrated solid immersion lenses," Appl. Phys. Lett. **97**, 241901 (2010).
25. A. Faraon, P. E. Barclay, C. Santori, K.-M. C. Fu, and R. G. Beausoleil, "Resonant enhancement of the zero-phonon emission from a colour centre in a diamond cavity," Nat. Photonics **5**, 301–305 (2011).
26. J. Riedrich-Möller, L. Kipfstuhl, C. Hepp, E. Neu, C. Pauly, F. Mücklich, A. Baur, M. Wandt, S. Wolff, M. Fischer, S. Gsell, M. Schreck, and C. Becher, "One- and two-dimensional photonic crystal microcavities in single crystal diamond," Nat. Nanotechnol. **7**, 69–74 (2012).
27. L. Li, T. Schröder, E. H. Chen, M. Walsh, I. Bayn, J. Goldstein, O. Gaathon, M. E. Trusheim, M. Lu, J. Mower, M. Cotlet, M. L. Markham, D. J. Twitchen, and D. Englund, "Coherent spin control of a nanocavity-enhanced qubit in diamond," Nat. Commun. **6**, 6173 (2015).
28. I. Bayn, B. Meyler, J. Salzman, and R. Kalish, "Triangular nanobeam photonic cavities in single-crystal diamond," New J. Phys. **13**, 025018 (2011).
29. Y. Ando, Y. Nishibayashi, K. Kobashi, T. Hirao, and K. Oura, "Smooth and high-rate reactive ion etching of diamond," Diam. Relat. Mater. **11**, 824–827 (2002).
30. B. J. M. Hausmann, M. Khan, Y. Zhang, T. M. Babinec, K. Martinick, M. McCutcheon, P. R. Hemmer, and M. Lončar, "Fabrication of diamond nanowires for quantum information processing applications," Diam. Relat. Mater. **19**, 621–629 (2010).
31. L. Li, I. Bayn, M. Lu, C.-Y. Nam, T. Schröder, A. Stein, N. C. Harris, and D. Englund, "Nanofabrication on unconventional substrates using transferred hard masks," Sci. Rep. **5**, 7802 (2015).
32. B. Khanaliloo, M. Mitchell, A. C. Hryciw, and P. E. Barclay, "High-Q/V monolithic diamond microdisks fabricated with quasi-isotropic etching," Nano Lett. **15**, 5131–5136 (2015).
33. A. A. Martin, M. Toth, and I. Aharonovich, "Subtractive 3D printing of optically active diamond structures," Sci. Rep. **4**, 5022 (2014).

34. S. Schietinger, M. Barth, T. Aichele, and O. Benson, "Plasmon-enhanced single photon emission from a nanoassembled metal–diamond hybrid structure at room temperature," Nano Lett. **9**, 1694–1698 (2009).
35. M. Barth, S. Schietinger, T. Schröder, T. Aichele, and O. Benson, "Controlled coupling of NV defect centers to plasmonic and photonic nanostructures," J. Lumin. **130**, 1628–1634 (2010).
36. I. Bulu, T. Babinec, B. Hausmann, J. T. Choy, and M. Lončar, "Plasmonic resonators for enhanced diamond NV- center single photon sources," Opt. Express **19**, 5268 (2011).
37. J. T. Choy, I. Bulu, B. J. M. Hausmann, E. Janitz, I.-C. Huang, and M. Lončar, "Spontaneous emission and collection efficiency enhancement of single emitters in diamond via plasmonic cavities and gratings," Appl. Phys. Lett. **103**, 161101 (2013).
38. B. J. M. Hausmann, I. Bulu, V. Venkataraman, P. Deotare, and M. Lončar, "Diamond nonlinear photonics," Nat. Photonics **8**, 369–374 (2014).
39. R. P. Mildren and A. Sabella, "Highly efficient diamond Raman laser," Opt. Lett. **34**, 2811–2813 (2009).
40. P. Ovartchaiyapong, L. M. A. Pascal, B. A. Myers, P. Lauria, and A. C. B. Jayich, "High quality factor single-crystal diamond mechanical resonators," Appl. Phys. Lett. **101**, 163505 (2012).
41. O. Benson, "Assembly of hybrid photonic architectures from nanophotonic constituents," Nature **480**, 193–199 (2011).
42. M. E. Trusheim, L. Li, A. Laraoui, E. H. Chen, H. Bakhru, T. Schröder, O. Gaathon, C. A. Meriles, and D. Englund, "Scalable fabrication of high purity diamond nanocrystals with long-spin-coherence nitrogen vacancy centers," Nano Lett. **14**, 32–36 (2014).
43. H. S. Knowles, D. M. Kara, and M. Atatüre, "Observing bulk diamond spin coherence in high-purity nanodiamonds," Nat. Mater. **13**, 21–25 (2014).
44. C. J. H. Wort and R. S. Balmer, "Diamond as an electronic material," Mater. Today **11**(1–2), 22–28 (2008).
45. R. S. Balmer, J. R. Brandon, S. L. Clewes, H. K. Dhillon, J. M. Dodson, I. Friel, P. N. Inglis, T. D. Madgwick, M. L. Markham, T. P. Mollart, N. Perkins, G. A. Scarsbrook, D. J. Twitchen, A. J. Whitehead, J. J. Wilman, and S. M. Woollard, "Chemical vapour deposition synthetic diamond: materials, technology and applications," J. Phys. **21**, 364221 (2009).
46. V. N. Mochalin, O. Shenderova, D. Ho, and Y. Gogotsi, "The properties and applications of nanodiamonds," Nat. Nanotechnol. **7**, 11–23 (2012).
47. J. E. Desnoyehs and J. A. Morrison, "The heat capacity of diamond between 12·8° and 277°K," Philos. Mag. **3**(25), 42–48 (1958).
48. G. Balasubramanian, P. Neumann, D. Twitchen, M. Markham, R. Kolesov, N. Mizuochi, J. Isoya, J. Achard, J. Beck, J. Tissler, V. Jacques, P. R. Hemmer, F. Jelezko, and J. Wrachtrup, "Ultralong spin coherence time in isotopically engineered diamond," Nat. Mater. **8**, 383–387 (2009).
49. T. Teraji, T. Taniguchi, S. Koizumi, K. Watanabe, M. Liao, Y. Koide, and J. Isoya, "Chemical vapor deposition of 12 C isotopically enriched polycrystalline diamond," Jpn. J. Appl. Phys. **51**, 090104 (2012).
50. A. M. Zaitsev, *Optical Properties of Diamond* (Springer, 2001).
51. I. Aharonovich and E. Neu, "Diamond nanophotonics," Adv. Opt. Mater. **2**, 911–928 (2014).
52. A. Gruber, A. Dräbenstedt, C. Tietz, L. Fleury, J. Wrachtrup, and C. V. Borczyskowski, "Scanning confocal optical microscopy and magnetic resonance on single defect centers," Science **276**, 2012–2014 (1997).
53. H. J. Kimble, "The quantum internet," Nature **453**, 1023–1030 (2008).
54. D. D. Awschalom, L. C. Bassett, A. S. Dzurak, E. L. Hu, and J. R. Petta, "Quantum spintronics: engineering and manipulating atom-like spins in semiconductors," Science **339**, 1174–1179 (2013).
55. M. W. Doherty, N. B. Manson, P. Delaney, F. Jelezko, J. Wrachtrup, and L. C. L. Hollenberg, "The nitrogen-vacancy colour centre in diamond," Phys. Rep. **528**, 1–45 (2013).
56. E. Togan, Y. Chu, A. S. Trifonov, L. Jiang, J. Maze, L. Childress, M. V. G. Dutt, A. S. Sørensen, P. R. Hemmer, A. S. Zibrov, and M. D. Lukin, "Quantum entanglement between an optical photon and a solid-state spin qubit," Nature **466**, 730–734 (2010).
57. H. Bernien, B. Hensen, W. Pfaff, G. Koolstra, M. S. Blok, L. Robledo, T. H. Taminiau, M. Markham, D. J. Twitchen, L. Childress, and R. Hanson, "Heralded entanglement between solid-state qubits separated by three metres," Nature **497**, 86–90 (2013).
58. W. Pfaff, B. J. Hensen, H. Bernien, S. B. V. Dam, M. S. Blok, T. H. Taminiau, M. J. Tiggelman, R. N. Schouten, M. Markham, D. J. Twitchen, and R. Hanson, "Unconditional quantum teleportation between distant solid-state quantum bits," Science **345**, 532–535 (2014).
59. B. Hensen, H. Bernien, A. E. Dréau, A. Reiserer, N. Kalb, M. S. Blok, J. Ruitenberg, R. F. L. Vermeulen, R. N. Schouten, C. Abellán, W. Amaya, V. Pruneri, M. W. Mitchell, M. Markham, D. J. Twitchen, D. Elkouss, S. Wehner, T. H. Taminiau, and R. Hanson, "Loophole-free Bell inequality violation using electron spins separated by 1.3 kilometres," Nature **526**, 682–686 (2015).
60. H. Kosaka and N. Niikura, "Entangled absorption of a single photon with a single spin in diamond," Phys. Rev. Lett. **114**, 053603 (2015).
61. R. Yang, C. A. Zorman, and P. X. L. Feng, "High frequency torsional-mode nanomechanical resonators enabled by very thin nanocrystalline diamond diaphragms," Diam. Relat. Mater. **54**, 19–25 (2015).
62. A. Sipahigil, K. Jahnke, L. Rogers, T. Teraji, J. Isoya, A. Zibrov, F. Jelezko, and M. Lukin, "Indistinguishable photons from separated silicon-vacancy centers in diamond," Phys. Rev. Lett. **113**, 113602 (2014).
63. S. Furuyama, K. Tahara, T. Iwasaki, M. Shimizu, J. Yaita, M. Kondo, T. Kodera, and M. Hatano, "Improvement of fluorescence intensity of nitrogen vacancy centers in self-formed diamond microstructures," Appl. Phys. Lett. **107**, 163102 (2015).
64. I. Aharonovich, J. C. Lee, A. P. Magyar, D. O. Bracher, and E. L. Hu, "Bottom-up engineering of diamond micro- and nano-structures," Laser Photon. Rev. **7**, L61–L65 (2013).
65. D. Sovyk, V. Ralchenko, M. Komlenok, A. A. Khomich, V. Shershulin, V. Vorobyov, I. Vlasov, V. Konov, and A. Akimov, "Fabrication of diamond microstub photoemitters with strong photoluminescence of SiV color centers: bottom-up approach," Appl. Phys. A **118**, 17–21 (2014).
66. Y. Tao and C. Degen, "Facile fabrication of single-crystal-diamond nanostructures with ultrahigh aspect ratio," Adv. Mater. **25**, 3962–3967 (2013).
67. I. Bayn, B. Meyler, A. Lahav, J. Salzman, R. Kalish, B. A. Fairchild, S. Prawer, M. Barth, O. Benson, T. Wolf, P. Siyushev, F. Jelezko, and J. Wrachtrup, "Processing of photonic crystal nanocavity for quantum information in diamond," Diam. Relat. Mater. **20**, 937–943 (2011).
68. M. Lesik, P. Spinicelli, S. Pezzagna, P. Happel, V. Jacques, O. Salord, B. Rasser, A. Delobbe, P. Sudraud, A. Tallaire, J. Meijer, and J.-F. Roch, "Maskless and targeted creation of arrays of colour centres in diamond using focused ion beam technology," Phys. Status Solidi A **210**, 2055–2059 (2013).
69. M. J. Burek, N. P. de Leon, B. J. Shields, B. J. M. Hausmann, Y. Chu, Q. Quan, A. S. Zibrov, H. Park, M. D. Lukin, and M. Lončar, "Free-standing mechanical and photonic nanostructures in single-crystal diamond," Nano Lett. **12**, 6084–6089 (2012).
70. M. J. Burek, Y. Chu, M. S. Z. Liddy, P. Patel, J. Rochman, S. Meesala, W. Hong, Q. Quan, M. D. Lukin, and M. Lončar, "High quality-factor optical nanocavities in bulk single-crystal diamond," Nat. Commun. **5**, 5718 (2014).
71. B. Khanaliloo, H. Jayakumar, A. C. Hryciw, D. P. Lake, H. Kaviani, and P. E. Barclay, "Single-crystal diamond nanobeam waveguide optomechanics," Phys. Rev. X **5**, 041051 (2015).
72. M. Schreck, J. Asmussen, S. Shikata, J.-C. Arnault, and N. Fujimori, "Large-area high-quality single crystal diamond," MRS Bull. **39**(06), 504–510 (2014).
73. T. A. Kennedy, J. S. Colton, J. E. Butler, R. C. Linares, and P. J. Doering, "Long coherence times at 300 K for nitrogen-vacancy center spins in diamond grown by chemical vapor deposition," Appl. Phys. Lett. **83**, 4190–4192 (2003).
74. K. Ohno, F. J. Heremans, L. C. Bassett, B. A. Myers, D. M. Toyli, A. C. B. Jayich, C. J. Palmstrøm, and D. D. Awschalom, "Engineering shallow spins in diamond with nitrogen delta-doping," Appl. Phys. Lett. **101**, 082413 (2012).

75. L. J. Rogers, K. D. Jahnke, T. Teraji, L. Marseglia, C. Müller, B. Naydenov, H. Schauffert, C. Kranz, J. Isoya, L. P. McGuinness, and F. Jelezko, "Multiple intrinsically identical single-photon emitters in the solid state," Nat. Commun. **5**, 4739 (2014).
76. J. C. Lee, D. O. Bracher, S. Cui, K. Ohno, C. A. McLellan, X. Zhang, P. Andrich, B. Alemán, K. J. Russell, A. P. Magyar, I. Aharonovich, A. B. Jayich, D. Awschalom, and E. L. Hu, "Deterministic coupling of delta-doped nitrogen vacancy centers to a nanobeam photonic crystal cavity," Appl. Phys. Lett. **105**, 261101 (2014).
77. T. Teraji, T. Yamamoto, K. Watanabe, Y. Koide, J. Isoya, S. Onoda, T. Ohshima, L. J. Rogers, F. Jelezko, P. Neumann, J. Wrachtrup, and S. Koizumi, "Homoepitaxial diamond film growth: high purity, high crystalline quality, isotopic enrichment, and single color center formation," Phys. Status Solidi A **212**, 2365–2384 (2015).
78. S. Gsell, T. Bauer, J. Goldfuß, M. Schreck, and B. Stritzker, "A route to diamond wafers by epitaxial deposition on silicon via iridium/yttria-stabilized zirconia buffer layers," Appl. Phys. Lett. **84**, 4541–4543 (2004).
79. M. Schreck, F. Hörmann, H. Roll, J. K. N. Lindner, and B. Stritzker, "Diamond nucleation on iridium buffer layers and subsequent textured growth: a route for the realization of single-crystal diamond films," Appl. Phys. Lett. **78**, 192–194 (2001).
80. M. Schreck, A. Schury, F. Hörmann, H. Roll, and B. Stritzker, "Mosaicity reduction during growth of heteroepitaxial diamond films on iridium buffer layers: experimental results and numerical simulations," J. Appl. Phys. **91**, 676–685 (2002).
81. P. Olivero, S. Rubanov, P. Reichart, B. C. Gibson, S. T. Huntington, J. R. Rabeau, A. D. Greentree, J. Salzman, D. Moore, D. N. Jamieson, and S. Prawer, "Characterization of three-dimensional microstructures in single-crystal diamond," Diam. Relat. Mater. **15**, 1614–1621 (2006).
82. L. Li, M. Trusheim, O. Gaathon, K. Kisslinger, C.-J. Cheng, M. Lu, D. Su, X. Yao, H.-C. Huang, I. Bayn, A. Wolcott, R. M. Osgood, Jr., and D. Englund, "Reactive ion etching: optimized diamond membrane fabrication for transmission electron microscopy," J. Vac. Sci. Technol. B **31**, 06FF01 (2013).
83. J. S. Hodges, L. Li, M. Lu, E. H. Chen, M. E. Trusheim, S. Allegri, X. Yao, O. Gaathon, H. Bakhru, and D. Englund, "Long-lived NV-spin coherence in high-purity diamond membranes," New J. Phys. **14**, 093004 (2012).
84. C. F. Wang, R. Hanson, D. D. Awschalom, E. L. Hu, T. Feygelson, J. Yang, and J. E. Butler, "Fabrication and characterization of two-dimensional photonic crystal microcavities in nanocrystalline diamond," Appl. Phys. Lett. **91**, 201112 (2007).
85. B. A. Fairchild, P. Olivero, S. Rubanov, A. D. Greentree, F. Waldermann, R. A. Taylor, I. Walmsley, J. M. Smith, S. Huntington, B. C. Gibson, D. N. Jamieson, and S. Prawer, "Fabrication of ultrathin single-crystal diamond membranes," Adv. Mater. **20**, 4793–4798 (2008).
86. A. P. Magyar, J. C. Lee, A. M. Limarga, I. Aharonovich, F. Rol, D. R. Clarke, M. Huang, and E. L. Hu, "Fabrication of thin, luminescent, single-crystal diamond membranes," Appl. Phys. Lett. **99**, 081913 (2011).
87. J. C. Lee, A. P. Magyar, D. O. Bracher, I. Aharonovich, and E. L. Hu, "Fabrication of thin diamond membranes for photonic applications," Diam. Relat. Mater. **33**, 45–48 (2013).
88. I. Aharonovich, J. C. Lee, A. P. Magyar, B. B. Buckley, C. G. Yale, D. D. Awschalom, and E. L. Hu, "Homoepitaxial growth of single crystal diamond membranes for quantum information processing," Adv. Mater. **24**, OP54–OP59 (2012).
89. O. Gaathon, J. S. Hodges, E. H. Chen, L. Li, S. Bakhru, H. Bakhru, D. Englund, and R. M. Osgood, Jr., "Planar fabrication of arrays of ion-exfoliated single-crystal-diamond membranes with nitrogen-vacancy color centers," Opt. Mater. **35**, 361–365 (2013).
90. A. A. Martin, S. Randolph, A. Botman, M. Toth, and I. Aharonovich, "Maskless milling of diamond by a focused oxygen ion beam," Sci. Rep. **5**, 8958 (2015).
91. J. T. Choy, B. J. M. Hausmann, T. M. Babinec, I. Bulu, M. Khan, P. Maletinsky, A. Yacoby, and M. Lončar, "Enhanced single-photon emission from a diamond-silver aperture," Nat. Photonics **5**, 738–743 (2011).
92. J. K. W. Yang, V. Anant, and K. K. Berggren, "Enhancing etch resistance of hydrogen silsesquioxane via postdevelop electron curing," J. Vac. Sci. Technol. B **24**, 3157 (2006).
93. M. Lipson, "Silicon photonics: an exercise in self control," Nat. Photonics **1**, 18–19 (2007).
94. X. Liu, R. M. Osgood, Y. A. Vlasov, and W. M. J. Green, "Mid-infrared optical parametric amplifier using silicon nanophotonic waveguides," Nat. Photonics **4**, 557–560 (2010).
95. C. Peroz, S. Dhuey, M. Cornet, M. Vogler, D. Olynick, and S. Cabrini, "Single digit nanofabrication by step-and-repeat nanoimprint lithography," Nanotechnology **23**, 015305 (2012).
96. I. Bayn, S. Mouradian, L. Li, J. A. Goldstein, T. Schröder, J. Zheng, E. H. Chen, O. Gaathon, M. Lu, A. Stein, C. A. Ruggiero, J. Salzman, R. Kalish, and D. Englund, "Fabrication of triangular nanobeam waveguide networks in bulk diamond using single-crystal silicon hard masks," Appl. Phys. Lett. **105**, 211101 (2014).
97. R. U. A. Khan, B. L. Cann, P. M. Martineau, J. Samartseva, J. J. P. Freeth, S. J. Sibley, C. B. Hartland, M. E. Newton, H. K. Dhillon, and D. J. Twitchen, "Colour-causing defects and their related optoelectronic transitions in single crystal CVD diamond," J. Phys. **25**, 275801 (2013).
98. J. Martin, R. Wannemacher, J. Teichert, L. Bischoff, and B. Köhler, "Generation and detection of fluorescent color centers in diamond with submicron resolution," Appl. Phys. Lett. **75**, 3096–3098 (1999).
99. C. Yang, D. N. Jamieson, C. Pakes, S. Prawer, A. Dzurak, F. Stanley, P. Spizziri, L. Macks, E. Gauja, and R. G. Clark, "Single phosphorus ion implantation into prefabricated nanometre cells of silicon devices for quantum bit fabrication," Jpn. J. Appl. Phys. **42**, 4124–4128 (2003).
100. C. A. McLellan, B. A. Myers, S. Kraemer, K. Ohno, D. D. Awschalom, and A. C. B. Jayich, "Deterministic formation of highly coherent nitrogen-vacancy centers using a focused electron irradiation technique," arXiv:1512.08821 [cond-mat] (2015).
101. I. Bayn, E. H. Chen, M. E. Trusheim, L. Li, T. Schröder, O. Gaathon, M. Lu, A. Stein, M. Liu, K. Kisslinger, H. Clevenson, and D. Englund, "Generation of ensembles of individually resolvable nitrogen vacancies using nanometer-scale apertures in ultrahigh-aspect ratio planar implantation masks," Nano Lett. **15**, 1751–1758 (2015).
102. G. Davies, "Charge states of the vacancy in diamond," Nature **269**, 498–500 (1977).
103. V. M. Acosta, E. Bauch, M. P. Ledbetter, C. Santori, K.-M. C. Fu, P. E. Barclay, R. G. Beausoleil, H. Linget, J. F. Roch, F. Treussart, S. Chemerisov, W. Gawlik, and D. Budker, "Diamonds with a high density of nitrogen-vacancy centers for magnetometry applications," Phys. Rev. B **80**, 115202 (2009).
104. S. Pezzagna, B. Naydenov, F. Jelezko, J. Wrachtrup, and J. Meijer, "Creation efficiency of nitrogen-vacancy centres in diamond," New J. Phys. **12**, 065017 (2010).
105. J. O. Orwa, C. Santori, K. M. C. Fu, B. Gibson, D. Simpson, I. Aharonovich, A. Stacey, A. Cimmino, P. Balog, M. Markham, D. Twitchen, A. D. Greentree, R. G. Beausoleil, and S. Prawer, "Engineering of nitrogen-vacancy color centers in high purity diamond by ion implantation and annealing," J. Appl. Phys. **109**, 083530 (2011).
106. G. Davies and M. F. Hamer, "Optical studies of the 1.945 eV vibronic band in diamond," Proc. R. Soc. London A **348**, 285–298 (1976).
107. A. T. Collins and I. Kiflawi, "The annealing of radiation damage in type Ia diamond," J. Phys. **21**, 364209 (2009).
108. P. Deák, B. Aradi, M. Kaviani, T. Frauenheim, and A. Gali, "Formation of NV centers in diamond: a theoretical study based on calculated transitions and migration of nitrogen and vacancy related defects," Phys. Rev. B **89**, 075203 (2014).
109. J. Schwartz, S. Aloni, D. F. Ogletree, and T. Schenkel, "Effects of low-energy electron irradiation on formation of nitrogen-vacancy centers in single-crystal diamond," New J. Phys. **14**, 043024 (2012).
110. J. Schwartz, S. Aloni, D. F. Ogletree, M. Tomut, M. Bender, D. Severin, C. Trautmann, I. W. Rangelow, and T. Schenkel, "Local formation of nitrogen-vacancy centers in diamond by swift heavy ions," J. Appl. Phys. **116**, 214107 (2014).

111. C. Santori, P. E. Barclay, K.-M. C. Fu, and R. G. Beausoleil, "Vertical distribution of nitrogen-vacancy centers in diamond formed by ion implantation and annealing," Phys. Rev. B **79**, 125313 (2009).
112. K. Ohno, F. J. Heremans, C. F. D. l. Casas, B. A. Myers, B. J. Alemán, A. C. B. Jayich, and D. D. Awschalom, "Three-dimensional localization of spins in diamond using 12c implantation," Appl. Phys. Lett. **105**, 052406 (2014).
113. B. Naydenov, F. Reinhard, A. Lämmle, V. Richter, R. Kalish, U. F. S. D'Haenens-Johansson, M. Newton, F. Jelezko, and J. Wrachtrup, "Increasing the coherence time of single electron spins in diamond by high temperature annealing," Appl. Phys. Lett. **97**, 242511 (2010).
114. R. E. Evans, A. Sipahigil, D. D. Sukachev, A. S. Zibrov, and M. D. Lukin, "Coherent optical emitters in diamond nanostructures via ion implantation," arXiv:1512.03820 [cond-mat, physics:quant-ph] (2015).
115. Y. Chu, N. de Leon, B. Shields, B. Hausmann, R. Evans, E. Togan, M. J. Burek, M. Markham, A. Stacey, A. Zibrov, A. Yacoby, D. Twitchen, M. Lončar, H. Park, P. Maletinsky, and M. Lukin, "Coherent optical transitions in implanted nitrogen vacancy centers," Nano Lett. **14**, 1982–1986 (2014).
116. P. Tamarat, T. Gaebel, J. R. Rabeau, M. Khan, A. D. Greentree, H. Wilson, L. C. L. Hollenberg, S. Prawer, P. Hemmer, F. Jelezko, and J. Wrachtrup, "Stark shift control of single optical centers in diamond," Phys. Rev. Lett. **97**, 083002 (2006).
117. S. Cui and E. L. Hu, "Effect of fluorinated diamond surface on charge state of nitrogen-vacancy centers," arXiv:1304.1407 (2013).
118. A. Mainwood, "Nitrogen and nitrogen-vacancy complexes and their formation in diamond," Phys. Rev. B **49**, 7934–7940 (1994).
119. F. C. Waldermann, P. Olivero, J. Nunn, K. Surmacz, Z. Y. Wang, D. Jaksch, R. A. Taylor, I. A. Walmsley, M. Draganski, P. Reichart, A. D. Greentree, D. N. Jamieson, and S. Prawer, "Creating diamond color centers for quantum optical applications," Diam. Relat. Mater. **16**, 1887–1895 (2007).
120. Z. Huang, W.-D. Li, C. Santori, V. M. Acosta, A. Faraon, T. Ishikawa, W. Wu, D. Winston, R. S. Williams, and R. G. Beausoleil, "Diamond nitrogen-vacancy centers created by scanning focused helium ion beam and annealing," Appl. Phys. Lett. **103**, 081906 (2013).
121. D. McCloskey, D. Fox, N. O'Hara, V. Usov, D. Scanlan, N. McEvoy, G. S. Duesberg, G. L. W. Cross, H. Z. Zhang, and J. F. Donegan, "Helium ion microscope generated nitrogen-vacancy centres in type Ib diamond," Appl. Phys. Lett. **104**, 031109 (2014).
122. P. Andrich, B. J. Alemán, J. C. Lee, K. Ohno, C. F. de las Casas, F. J. Heremans, E. L. Hu, and D. D. Awschalom, "Engineered micro- and nanoscale diamonds as mobile probes for high-resolution sensing in fluid," Nano Lett. **14**, 4959–4964 (2014).
123. T. Gaebel, M. Domhan, I. Popa, C. Wittmann, P. Neumann, F. Jelezko, J. R. Rabeau, N. Stavrias, A. D. Greentree, S. Prawer, J. Meijer, J. Twamley, P. R. Hemmer, and J. Wrachtrup, "Room-temperature coherent coupling of single spins in diamond," Nat. Phys. **2**, 408–413 (2006).
124. J. Cai, A. Retzker, F. Jelezko, and M. B. Plenio, "A large-scale quantum simulator on a diamond surface at room temperature," Nat. Phys. **9**, 168–173 (2013).
125. G. Waldherr, Y. Wang, S. Zaiser, M. Jamali, T. Schulte-Herbrüggen, H. Abe, T. Ohshima, J. Isoya, J. F. Du, P. Neumann, and J. Wrachtrup, "Quantum error correction in a solid-state hybrid spin register," Nature **506**, 204–207 (2014).
126. T. H. Taminiau, J. Cramer, T. V. D. Sar, V. V. Dobrovitski, and R. Hanson, "Universal control and error correction in multi-qubit spin registers in diamond," Nat. Nanotechnol. **9**, 171–176 (2014).
127. J. Meijer, B. Burchard, M. Domhan, C. Wittmann, T. Gaebel, I. Popa, F. Jelezko, and J. Wrachtrup, "Generation of single color centers by focused nitrogen implantation," Appl. Phys. Lett. **87**, 261909 (2005).
128. J. R. Rabeau, P. Reichart, G. Tamanyan, D. N. Jamieson, S. Prawer, F. Jelezko, T. Gaebel, I. Popa, M. Domhan, and J. Wrachtrup, "Implantation of labelled single nitrogen vacancy centers in diamond using N15," Appl. Phys. Lett. **88**, 023113 (2006).
129. S. Pezzagna, D. Rogalla, D. Wildanger, J. Meijer, and A. Zaitsev, "Creation and nature of optical centres in diamond for single-photon emission-overview and critical remarks," New J. Phys. **13**, 035024 (2011).
130. J. F. Ziegler and J. P. Biersack, "The stopping and range of ions in matter," in *Treatise on Heavy-Ion Science*, D. A. Bromley, ed. (Springer, 1985), pp. 93–129.
131. J. Ziegler, Interactions of Ions with Matter, http://srim.org/.
132. C. Wang, C. Kurtsiefer, H. Weinfurter, and B. Burchard, "Single photon emission from SiV centres in diamond produced by ion implantation," J. Phys. B **39**, 37–41 (2006).
133. D. Antonov, T. Häußermann, A. Aird, J. Roth, H.-R. Trebin, C. Müller, L. McGuinness, F. Jelezko, T. Yamamoto, J. Isoya, S. Pezzagna, J. Meijer, and J. Wrachtrup, "Statistical investigations on nitrogen-vacancy center creation," Appl. Phys. Lett. **104**, 012105 (2014).
134. J. Meijer, S. Pezzagna, T. Vogel, B. Burchard, H. H. Bukow, I. W. Rangelow, Y. Sarov, H. Wiggers, I. Plümel, F. Jelezko, J. Wrachtrup, F. Schmidt-Kaler, W. Schnitzler, and K. Singer, "Towards the implanting of ions and positioning of nanoparticles with nm spatial resolution," Appl. Phys. A **91**, 567–571 (2008).
135. K. Y. Han, K. I. Willig, E. Rittweger, F. Jelezko, C. Eggeling, and S. W. Hell, "Three-dimensional stimulated emission depletion microscopy of nitrogen-vacancy centers in diamond using continuous-wave light," Nano Lett. **9**, 3323–3329 (2009).
136. S. Pezzagna, D. Wildanger, P. Mazarov, A. D. Wieck, Y. Sarov, I. Rangelow, B. Naydenov, F. Jelezko, S. W. Hell, and J. Meijer, "Nanoscale engineering and optical addressing of single spins in diamond," Small **6**, 2117–2121 (2010).
137. D. M. Toyli, C. D. Weis, G. D. Fuchs, T. Schenkel, and D. D. Awschalom, "Chip-scale nanofabrication of single spins and spin arrays in diamond," Nano Lett. **10**, 3168–3172 (2010).
138. S. Tamura, G. Koike, A. Komatsubara, T. Teraji, S. Onoda, L. P. McGuinness, L. Rogers, B. Naydenov, E. Wu, L. Yan, F. Jelezko, T. Ohshima, J. Isoya, T. Shinada, and T. Tanii, "Array of bright silicon-vacancy centers in diamond fabricated by low-energy focused ion beam implantation," Appl. Phys. Express **7**, 115201 (2014).
139. J. Riedrich-Möller, C. Arend, C. Pauly, F. Mücklich, M. Fischer, S. Gsell, M. Schreck, and C. Becher, "Deterministic coupling of a single silicon-vacancy color center to a photonic crystal cavity in diamond," Nano Lett. **14**, 5281–5287 (2014).
140. J. Riedrich-Möller, S. Pezzagna, J. Meijer, C. Pauly, F. Mücklich, M. Markham, A. M. Edmonds, and C. Becher, "Nanoimplantation and Purcell enhancement of single nitrogen-vacancy centers in photonic crystal cavities in diamond," Appl. Phys. Lett. **106**, 221103 (2015).
141. T. Schröder, E. Chen, L. Li, M. Walsh, M. E. Trusheim, I. Bayn, and D. Englund, "Targeted creation and Purcell enhancement of NV centers within photonic crystal cavities in single-crystal diamond," in *Conference on Lasers and Electro-Optics*, OSA Technical Digest (online) (Optical Society of America, 2014), paper FW1B.6.
142. T. Schröder, L. Li, E. Chen, M. Walsh, M. E. Trusheim, I. Bayn, J. Zheng, S. Mouradian, H. Bakhru, O. Gaathon, and D. R. Englund, "Deterministic high-yield creation of nitrogen vacancy centers in diamond photonic crystal cavities and photonic elements," in *Conference on Lasers and Electro-Optics*, OSA Technical Digest (online) (Optical Society of America, 2015), paper FTh3B.1.
143. A. M. Edmonds, U. F. S. D'Haenens-Johansson, R. J. Cruddace, M. E. Newton, K.-M. C. Fu, C. Santori, R. G. Beausoleil, D. J. Twitchen, and M. L. Markham, "Production of oriented nitrogen-vacancy color centers in synthetic diamond," Phys. Rev. B **86**, 035201 (2012).
144. L. M. Pham, N. Bar-Gill, C. Belthangady, D. Le Sage, P. Cappellaro, M. D. Lukin, A. Yacoby, and R. L. Walsworth, "Enhanced solid-state multispin metrology using dynamical decoupling," Phys. Rev. B **86**, 045214 (2012).
145. J. Michl, T. Teraji, S. Zaiser, I. Jakobi, G. Waldherr, F. Dolde, P. Neumann, M. W. Doherty, N. B. Manson, J. Isoya, and J. Wrachtrup, "Perfect alignment and preferential orientation of nitrogen-vacancy centers during chemical vapor deposition diamond growth on (111) surfaces," Appl. Phys. Lett. **104**, 102407 (2014).
146. M. Lesik, J.-P. Tetienne, A. Tallaire, J. Achard, V. Mille, A. Gicquel, J.-F. Roch, and V. Jacques, "Perfect preferential orientation of nitrogen-vacancy defects in a synthetic diamond sample," Appl. Phys. Lett. **104**, 113107 (2014).

147. K. Nemoto, M. Trupke, S. J. Devitt, B. Scharfenberger, K. Buczak, J. Schmiedmayer, and W. J. Munro, "Photonic quantum networks formed from NV- centers," arXiv:1412.5950 [quant-ph] (2014).
148. B. Shields, Q. Unterreithmeier, N. de Leon, H. Park, and M. Lukin, "Efficient readout of a single spin state in diamond via spin-to-charge conversion," Phys. Rev. Lett. **114**, 136402 (2015).
149. W. Lukosz and R. E. Kunz, "Light emission by magnetic and electric dipoles close to a plane interface. I. Total radiated power," J. Opt. Soc. Am. **67**, 1607–1615 (1977).
150. K. G. Lee, X. W. Chen, H. Eghlidi, P. Kukura, R. Lettow, A. Renn, V. Sandoghdar, and S. Götzinger, "A planar dielectric antenna for directional single-photon emission and near-unity collection efficiency," Nat. Photonics **5**, 166–169 (2011).
151. T. Schröder, F. Gädeke, M. J. Banholzer, and O. Benson, "Ultrabright and efficient single-photon generation based on nitrogen-vacancy centres in nanodiamonds on a solid immersion lens," New J. Phys. **13**, 055017 (2011).
152. E. Neu, P. Appel, M. Ganzhorn, J. Miguel-Sánchez, M. Lesik, V. Mille, V. Jacques, A. Tallaire, J. Achard, and P. Maletinsky, "Photonic nano-structures on (111)-oriented diamond," Appl. Phys. Lett. **104**, 153108 (2014).
153. S. A. Momenzadeh, R. J. Stöhr, F. F. de Oliveira, A. Brunner, A. Denisenko, S. Yang, F. Reinhard, and J. Wrachtrup, "Nanoengineered diamond waveguide as a robust bright platform for nanomagnetometry using shallow nitrogen vacancy centers," Nano Lett. **15**, 165–169 (2015).
154. S. L. Mouradian, T. Schröder, C. B. Poitras, L. Li, J. Goldstein, E. H. Chen, M. Walsh, J. Cardenas, M. L. Markham, D. J. Twitchen, M. Lipson, and D. Englund, "Scalable integration of long-lived quantum memories into a photonic circuit," Phys. Rev. X **5**, 031009 (2015).
155. B. J. M. Hausmann, T. M. Babinec, J. T. Choy, J. S. Hodges, S. Hong, I. Bulu, A. Yacoby, M. D. Lukin, and M. Lončar, "Single-color centers implanted in diamond nanostructures," New J. Phys. **13**, 045004 (2011).
156. C. J. Widmann, C. Giese, M. Wolfer, D. Brink, N. Heidrich, and C. E. Nebel, "Fabrication and characterization of single crystalline diamond nanopillars with NV-centers," Diam. Relat. Mater. **54**, 2–8 (2015).
157. P. Maletinsky, S. Hong, M. S. Grinolds, B. Hausmann, M. D. Lukin, R. L. Walsworth, M. Lončar, and A. Yacoby, "A robust scanning diamond sensor for nanoscale imaging with single nitrogen-vacancy centres," Nature Nanotechnol. **7**, 320–324 (2012).
158. J. Love, W. Henry, W. Stewart, R. Black, S. Lacroix, and F. Gonthier, "Tapered single-mode fibres and devices. Part 1: adiabaticity criteria," IEE Proc. J. Optoelectron. **138**, 343–354 (1991).
159. M. Yoshita, K. Koyama, Y. Hayamizu, M. Baba, and H. Akiyama, "Improved high collection efficiency in fluorescence microscopy with a Weierstrass-sphere solid immersion lens," Jpn. J. Appl. Phys. **41**, L858–L860 (2002).
160. A. W. Schell, T. Neumer, and O. Benson, "Numerical analysis of efficient light extraction with an elliptical solid immersion lens," Opt. Lett. **39**, 4639–4642 (2014).
161. H. W. Choi, E. Gu, C. Liu, C. Griffin, J. M. Girkin, I. M. Watson, and M. D. Dawson, "Fabrication of natural diamond microlenses by plasma etching," J. Vac. Sci. Technol. B **23**, 130–132 (2005).
162. C. L. Lee, H. W. Choi, E. Gu, M. D. Dawson, and H. Murphy, "Fabrication and characterization of diamond micro-optics," Diam. Relat. Mater. **15**, 725–728 (2006).
163. L. Marseglia, J. P. Hadden, A. C. Stanley-Clarke, J. P. Harrison, B. Patton, Y.-L. D. Ho, B. Naydenov, F. Jelezko, J. Meijer, P. R. Dolan, J. M. Smith, J. G. Rarity, and J. L. O'Brien, "Nanofabricated solid immersion lenses registered to single emitters in diamond," Appl. Phys. Lett. **98**, 133107 (2011).
164. M. Jamali, I. Gerhardt, M. Rezai, K. Frenner, H. Fedder, and J. Wrachtrup, "Microscopic diamond solid-immersion-lenses fabricated around single defect centers by focused ion beam milling," Rev. Sci. Instrum. **85**, 123703 (2014).
165. C. Hepp, T. Müller, V. Waselowski, J. N. Becker, B. Pingault, H. Sternschulte, D. Steinmüller-Nethl, A. Gali, J. R. Maze, M. Atatüre, and C. Becher, "Electronic structure of the silicon vacancy color center in diamond," Phys. Rev. Lett. **112**, 036405 (2014).
166. P. Siyushev, F. Kaiser, V. Jacques, I. Gerhardt, S. Bischof, H. Fedder, J. Dodson, M. Markham, D. Twitchen, F. Jelezko, and J. Wrachtrup, "Monolithic diamond optics for single photon detection," Appl. Phys. Lett. **97**, 241902 (2010).
167. D. Riedel, D. Rohner, M. Ganzhorn, T. Kaldewey, P. Appel, E. Neu, R. Warburton, and P. Maletinsky, "Low-loss broadband antenna for efficient photon collection from a coherent spin in diamond," Phys. Rev. Appl. **2**, 064011 (2014).
168. L. Li, E. H. Chen, J. Zheng, S. L. Mouradian, F. Dolde, T. Schröder, S. Karaveli, M. L. Markham, D. J. Twitchen, and D. Englund, "Efficient photon collection from a nitrogen vacancy center in a circular bullseye grating," Nano Lett. **15**, 1493–1497 (2015).
169. A. Young, C. Y. Hu, L. Marseglia, J. P. Harrison, J. L. O'Brien, and J. G. Rarity, "Cavity enhanced spin measurement of the ground state spin of an NV center in diamond," New J. Phys. **11**, 013007 (2009).
170. K. J. Vahala, "Optical microcavities," Nature **424**, 839–846 (2003).
171. T. G. Tiecke, J. D. Thompson, N. P. de Leon, L. R. Liu, V. Vuletić, and M. D. Lukin, "Nanophotonic quantum phase switch with a single atom," Nature **508**, 241–244 (2014).
172. P. Meystre and M. Sargent, *Elements of Quantum Optics* (Springer, 2007).
173. E. M. Purcell, "Spontaneous emission probabilities at radio frequencies," Phys. Rev. **69**, 37–38 (1946).
174. C.-H. Su, A. D. Greentree, and L. C. L. Hollenberg, "Towards a picosecond transform-limited nitrogen-vacancy based single photon source," Opt. Express **16**, 6240–6250 (2008).
175. C.-H. Su, A. D. Greentree, and L. C. L. Hollenberg, "High-performance diamond-based single-photon sources for quantum communication," Phys. Rev. A **80**, 052308 (2009).
176. C. Santori, D. Fattal, and Y. Yamamoto, *Single-Photon Devices and Applications* (Wiley, 2010).
177. H.-Q. Zhao, M. Fujiwara, and S. Takeuchi, "Suppression of fluorescence phonon sideband from nitrogen vacancy centers in diamond nanocrystals by substrate effect," Opt. Express **20**, 15628 (2012).
178. C. F. Wang, Y.-S. Choi, J. C. Lee, E. L. Hu, J. Yang, and J. E. Butler, "Observation of whispering gallery modes in nanocrystalline diamond microdisks," Appl. Phys. Lett. **90**, 081110 (2007).
179. T. M. Babinec, J. T. Choy, K. J. M. Smith, M. Khan, and M. Lončar, "Design and focused ion beam fabrication of single crystal diamond nanobeam cavities," J. Vac. Sci. Technol. B **29**, 010601 (2011).
180. A. Faraon, Z. Huang, V. Acosta, C. Santori, and R. Beausoleil, "Coupling of nitrogen-vacancy centers to photonic crystal resonators in monocrystalline diamond," in *Conference on Lasers and Electro-Optics*, OSA Technical Digest (Optical Society of America, 2012), paper QM3C.5.
181. B. J. M. Hausmann, B. J. Shields, Q. Quan, Y. Chu, N. P. de Leon, R. Evans, M. J. Burek, A. S. Zibrov, M. Markham, D. J. Twitchen, H. Park, M. D. Lukin, and M. Lončar, "Coupling of NV centers to photonic crystal nanobeams in diamond," Nano Lett. **13**, 5791–5796 (2013).
182. I. Bayn, B. Meyler, J. Salzman, V. Richter, and R. Kalish, "Single crystal diamond photonic crystal nanocavity: fabrication and initial characterization," in *Conference on Lasers and Electro-Optics*, OSA Technical Digest (online) (Optical Society of America, 2010), paper QThL7.
183. B. J. M. Hausmann, B. Shields, Q. Quan, P. Maletinsky, M. McCutcheon, J. T. Choy, T. M. Babinec, A. Kubanek, A. Yacoby, M. D. Lukin, and M. Lončar, "Integrated diamond networks for quantum nanophotonics," Nano Lett. **12**, 1578–1582 (2012).
184. A. Faraon, C. Santori, Z. Huang, K.-M. C. Fu, V. M. Acosta, D. Fattal, and R. G. Beausoleil, "Quantum photonic devices in single-crystal diamond," New J. Phys. **15**, 025010 (2013).
185. B. J. M. Hausmann, I. B. Bulu, P. B. Deotare, M. McCutcheon, V. Venkataraman, M. L. Markham, D. J. Twitchen, and M. Lončar, "Integrated high-quality factor optical resonators in diamond," Nano Lett. **13**, 1898–1902 (2013).
186. Z. Huang, A. Faraon, C. Santori, V. Acosta, and R. G. Beausoleil, "Microring resonator-based diamond optothermal switch: a building

block for a quantum computing network," Proc. SPIE **8635**, 86350E (2013).
187. M. P. Hiscocks, K. Ganesan, B. C. Gibson, S. T. Huntington, F. Ladouceur, and S. Prawer, "Diamond waveguides fabricated by reactive ion etching," Opt. Express **16**, 19512–19519 (2008).
188. C. Santori, P. E. Barclay, K.-M. C. Fu, R. G. Beausoleil, S. Spillane, and M. Fisch, "Nanophotonics for quantum optics using nitrogen-vacancy centers in diamond," Nanotechnology **21**, 274008 (2010).
189. P. E. Barclay, K.-M. C. Fu, C. Santori, and R. G. Beausoleil, "Chip-based microcavities coupled to nitrogen-vacancy centers in single crystal diamond," Appl. Phys. Lett. **95**, 191115 (2009).
190. N. Thomas, R. J. Barbour, Y. Song, M. L. Lee, and K.-M. C. Fu, "Waveguide-integrated single-crystalline GaP resonators on diamond," Opt. Express **22**, 13555–13564 (2014).
191. P. E. Barclay, K.-M. C. Fu, C. Santori, A. Faraon, and R. G. Beausoleil, "Hybrid nanocavity resonant enhancement of color center emission in diamond," Phys. Rev. X **1**, 011007 (2011).
192. K.-M. C. Fu, P. E. Barclay, C. Santori, A. Faraon, and R. G. Beausoleil, "Low-temperature tapered-fiber probing of diamond nitrogen-vacancy ensembles coupled to GaP microcavities," New J. Phys. **13**, 055023 (2011).
193. M. Larsson, K. N. Dinyari, and H. Wang, "Composite optical microcavity of diamond nanopillar and silica microsphere," Nano Lett. **9**, 1447–1450 (2009).
194. M. Trupke, E. A. Hinds, S. Eriksson, E. A. Curtis, Z. Moktadir, E. Kukharenka, and M. Kraft, "Microfabricated high-finesse optical cavity with open access and small volume," Appl. Phys. Lett. **87**, 211106 (2005).
195. D. Hunger, C. Deutsch, R. J. Barbour, R. J. Warburton, and J. Reichel, "Laser micro-fabrication of concave, low-roughness features in silica," AIP Adv. **2**, 012119 (2012).
196. A. Muller, E. B. Flagg, J. R. Lawall, and G. S. Solomon, "Ultrahigh-finesse, low-mode-volume Fabry–Perot microcavity," Opt. Lett. **35**, 2293–2295 (2010).
197. P. R. Dolan, G. M. Hughes, F. Grazioso, B. R. Patton, and J. M. Smith, "Femtoliter tunable optical cavity arrays," Opt. Lett. **35**, 3556–3558 (2010).
198. T. Steinmetz, Y. Colombe, D. Hunger, T. W. Hänsch, A. Balocchi, R. J. Warburton, and J. Reichel, "Stable fiber-based Fabry–Pérot cavity," Appl. Phys. Lett. **89**, 111110 (2006).
199. R. Albrecht, A. Bommer, C. Deutsch, J. Reichel, and C. Becher, "Coupling of a single nitrogen-vacancy center in diamond to a fiber-based microcavity," Phys. Rev. Lett. **110**, 243602 (2013).
200. H. Kaupp, C. Deutsch, H.-C. Chang, J. Reichel, T. W. Hänsch, and D. Hunger, "Scaling laws of the cavity enhancement for NV centers in diamond," arXiv:1304.0948 (2013).
201. R. Albrecht, A. Bommer, C. Pauly, F. Mücklich, A. W. Schell, P. Engel, T. Schröder, O. Benson, J. Reichel, and C. Becher, "Narrow-band single photon emission at room temperature based on a single nitrogen-vacancy center coupled to an all-fiber-cavity," Appl. Phys. Lett. **105**, 073113 (2014).
202. E. Janitz, M. Ruf, M. Dimock, A. Bourassa, J. Sankey, and L. Childress, "Fabry–Perot microcavity for diamond-based photonics," Phys. Rev. A **92**, 043844 (2015).
203. K.-M. C. Fu, C. Santori, P. E. Barclay, I. Aharonovich, S. Prawer, N. Meyer, A. M. Holm, and R. G. Beausoleil, "Coupling of nitrogen-vacancy centers in diamond to a GaP waveguide," Appl. Phys. Lett. **93**, 234107 (2008).
204. P. E. Barclay, K.-M. Fu, C. Santori, and R. G. Beausoleil, "Hybrid photonic crystal cavity and waveguide for coupling to diamond NV-centers," Opt. Express **17**, 9588–9601 (2009).
205. M. Gould, S. Chakravarthi, I. R. Christen, N. Thomas, S. Dadgostar, Y. Song, M. L. Lee, F. Hatami, and K.-M. C. Fu, "A large-scale GaP-on-diamond integrated photonics platform for NV center-based quantum information," arXiv:1510.05047 [cond-mat, physics:physics, physics:quant-ph] (2015).
206. R. N. Patel, T. Schröder, N. Wan, L. Li, S. L. Mouradian, E. H. Chen, and D. R. Englund, "Efficient photon coupling from a diamond nitrogen vacancy center by integration with silica fiber," Light Sci. Appl. **5**, e16032 (2016).
207. J. P. Sprengers, A. Gaggero, D. Sahin, S. Jahanmirinejad, G. Frucci, F. Mattioli, R. Leoni, J. Beetz, M. Lermer, M. Kamp, S. Höfling, R. Sanjines, and A. Fiore, "Waveguide superconducting single-photon detectors for integrated quantum photonic circuits," Appl. Phys. Lett. **99**, 181110 (2011).
208. F. Najafi, J. Mower, N. C. Harris, F. Bellei, A. Dane, C. Lee, X. Hu, P. Kharel, F. Marsili, S. Assefa, K. K. Berggren, and D. Englund, "On-chip detection of non-classical light by scalable integration of single-photon detectors," Nat. Commun. **6**, 5873 (2015).
209. H. A. Atikian, A. Eftekharian, A. J. Salim, M. J. Burek, J. T. Choy, A. H. Majedi, and M. Lončar, "Superconducting nanowire single photon detector on diamond," Appl. Phys. Lett. **104**, 122602 (2014).
210. P. Rath, O. Kahl, S. Ferrari, F. Sproll, G. Lewes-Malandrakis, D. Brink, K. Ilin, M. Siegel, C. Nebel, and W. Pernice, "Superconducting single-photon detectors integrated with diamond nanophotonic circuits," Light Sci. Appl. **4**, e338 (2015).
211. L.-M. Duan and H. J. Kimble, "Scalable photonic quantum computation through cavity-assisted interactions," Phys. Rev. Lett. **92**, 127902 (2004).
212. L.-M. Duan, M. D. Lukin, J. I. Cirac, and P. Zoller, "Long-distance quantum communication with atomic ensembles and linear optics," Nature **414**, 413–418 (2001).
213. X. Chew, G. Zhou, F. S. Chau, and J. Deng, "Enhanced resonance tuning of photonic crystal nanocavities by integration of optimized near-field multitip nanoprobes," J. Nanophoton. **5**, 059503 (2011).
214. M. S. Blok, N. Kalb, A. Reiserer, T. H. Taminiau, and R. Hanson, "Towards quantum networks of single spins: analysis of a quantum memory with an optical interface in diamond," Faraday Discuss. **184**, 173–182 (2015).
215. F. Dolde, V. Bergholm, Y. Wang, I. Jakobi, B. Naydenov, S. Pezzagna, J. Meijer, F. Jelezko, P. Neumann, T. Schulte-Herbrüggen, J. Biamonte, and J. Wrachtrup, "High-fidelity spin entanglement using optimal control," Nat. Commun. **5**, 3371 (2014).
216. J. Cramer, N. Kalb, M. A. Rol, B. Hensen, M. S. Blok, M. Markham, D. J. Twitchen, R. Hanson, and T. H. Taminiau, "Repeated quantum error correction on a continuously encoded qubit by real-time feedback," arXiv:1508.01388 [cond-mat, physics:quant-ph] (2015).